A review of Birkeland current research using AMPERE

Chapter · March 2018

DOI: 10.1002/9781119324522.ch16

CITATIONS
56

READS
576

3 authors, including:

John C Coxon
Northumbria University
60 PUBLICATIONS **1,458** CITATIONS
SEE PROFILE

Steve Milan
University of Leicester
481 PUBLICATIONS **12,652** CITATIONS
SEE PROFILE

16

A Review of Birkeland Current Research Using AMPERE

John C. Coxon[1], Stephen E. Milan[2], and Brian J. Anderson[3]

ABSTRACT

We review research into the Birkeland currents (also known as field-aligned currents) that has been conducted using the Active Magnetosphere and Planetary Electrodynamics Response Experiment (AMPERE). We open with a short review of the history of research into the Birkeland current systems, before describing the conception of AMPERE and its roots in Iridium telecommunications satellite engineering telemetry data. We describe the difference between Iridium engineering telemetry data and AMPERE data, and review the work that has been done using both datasets. We review research into Regions 1 and 2 Birkeland current during geomagnetic storms and consequently the ways in which the currents are driven by the solar wind, before moving onto the substorm current wedge and discussing the present controversy over this phenomenon in AMPERE data. Ways in which AMPERE data can be used to examine ionospheric conductivity are detailed alongside ways in which AMPERE has contributed to empirical models of the coupled solar wind-magnetosphere-ionosphere system. Finally, we look to the future and speculate on the manner in which AMPERE may yet unlock the secrets of the magnetosphere.

16.1. INTRODUCTION

At the turn of the twentieth century, the existence of field-aligned currents (FACs) was proposed by the Norwegian scientist Kristian Birkeland [*Birkeland*, 1908, 1913]. They were proposed as a mechanism to link the ionosphere to the solar wind, in order to explain observations of magnetic perturbations and aurorae that he made at an observatory in the north of Norway. The existence of field-aligned currents was not immediately accepted by the scientific community, and proved controversial until their eventual detection some 50 years after Birkeland's proposal [*Zmuda et al.*, 1966]; as a result, field-aligned currents are often referred to as Birkeland currents, in his honor. An overview of the debate surrounding Birkeland currents can be found within the detailed historical account that opens this monograph [*Brekke*, Chapter 1, this volume].

The first detailed study of Birkeland current structure was conducted by *Iijima and Potemra* [1976, 1978], who split the Birkeland current system into two regions, both of

[1] *Department of Physics and Astronomy, University of Southampton, Southampton, UK*

[2] *Department of Physics and Astronomy, University of Leicester, Leicester, UK; Birkeland Centre for Space Science, University of Bergen, Bergen, Norway*

[3] *Applied Physics Laboratory, Johns Hopkins University, Laurel, Maryland, USA*

Electric Currents in Geospace and Beyond, *Geophysical Monograph 235*, First Edition.
Edited by Andreas Keiling, Octav Marghitu, and Michael Wheatland.

which flow in an oval above the ionosphere. The Region 1 (R1) current connects the ionosphere to the magnetopause (on the dayside and flanks), and to the current sheet (on the nightside); the R1 current oval encircles the polar cap. The Region 2 (R2) current connects to the partial ring current in the inner magnetosphere, and the oval lies equatorward of R1. These two regions of Birkeland current are often found during periods of magnetic reconnection on the dayside, and they are consistent with reconnection-driven ionospheric convection [e.g., *Cowley*, 2000; *Coxon et al*., 2014a]. During substorms, when reconnection occurs in the magnetotail, a magnetic bay is observed in the AL index [*Akasofu and Meng*, 1969], which is a result of a current flowing west in the ionosphere; this current is known as the substorm electrojet. Field-aligned currents (FACs) flow into and out of the ionosphere at either end of the electrojet, and these currents are collectively referred to as the substorm current wedge, or SCW [McPherron et al., 1973; *Clauer and McPherron*].

Results from the Active Magnetosphere and Planetary Electrodynamics Response Experiment (AMPERE) on the R1/R2 current system and the SCW will be reviewed in sections 16.3 and 16.4, respectively. In addition to research on these large-scale current systems, AMPERE has also contributed to the study of other current systems, which are briefly reviewed in section 16.5. We discuss the contributions of AMPERE to studies of ionospheric conductivity in section 16.6 and to modeling studies (both as a contribution to empirical models as a comparison to theoretical models) in section 16.7. Finally, in section 16.8, we look to the future.

16.2. ABOUT AMPERE

AMPERE was conceived to investigate the dynamics of the Birkeland currents using magnetometer data from the attitude control systems of the Iridium telecommunications satellite network [*Anderson et al*., 2014]. AMPERE allows for the currents during dayside driving and during a substorm to be examined globally, and an example of the progression of the current systems is shown in Figure 16.1, which shows R1 and R2 currents flowing in Figure 16.1a,b and which shows the presence of additional current in the 21-03 MLT sector after substorm onset (Fig. 16.1c), which is an example of the SCW.

Data from the Iridium spacecraft constellation were first used to investigate the Birkeland current density by *Anderson et al*. [2000], and following initiation of AMPERE by the National Science Foundation, modifications to the Iridium flight software enabled acquisition of the higher rate AMPERE data, which were first made available in December 2010 [*Burke et al*., 2011]. The Iridium constellation comprises 66 satellites in the communications network together with on-orbit spares, which orbit the Earth in six circular, polar, orbital planes at an altitude of 780 km and a longitudinal spacing of ~2 hr of MLT, although as the orbits do not pass directly above the poles, this can be 1–3 hr of MLT [*Murphy et al*., 2013]. There are 11 satellites per orbital plane in the communications network, and each orbit takes 104 min, such that it takes a satellite 9.5 min to move from its current position to the current position of the next satellite.

The use of magnetometer data from the Iridium avionics magnetometers [*Anderson et al*., 2000; Waters *et al*., 2001] used the original engineering telemetry (TLM) data from the satellites, which were originally for monitoring satellite system performance. The TLM packets were nominally acquired every ~200 s, so magnetometer samples were acquired with a separation of ~1400 km in the along-track direction. The latitude spacing between samples in the TLM magnetometer data was therefore almost 15°, at least three times the nominal latitude extent of the R1/R2 current system [cf. *Iijima and Potemra*, 1976]. As a result, studies with these TLM data required at least one hour of magnetometer samples to obtain even a coarse estimate of the magnetic signals of the Birkeland current system [cf. *Korth et al*., 2010]. Even at this low capability, the data were used successfully for a variety of studies and it was established that the current systems derived from Iridium TLM data are consistent with R1 and R2 currents flowing during southward IMF and NBZ currents flowing during northward IMF, with rotations due to B_Y; examples of the large-scale current systems are shown later in Figure 16.3 [*Anderson et al*., 2008].

The time intervals between the TLM data packets could not be decreased within the bandwidth or onboard storage constraints of the space vehicles. Yet, only by increasing the data sampling by at least an order of magnitude could the Iridium magnetometer data acquire enough data to resolve the large-scale currents on each pass to take advantage of the satellite constellation revisit time of only 9.5 min. To solve this problem, the Active Magnetosphere and Planetary Electrodynamics Response Experiment (AMPERE) was conceived to support the purchase of a new data stream of avionics magnetometer and vehicle attitude and position data. Figure 16.2 shows examples of data acquired in 10 min intervals for the Iridium TLM data and AMPERE standard and high rate sampling. Unlike the Iridium TLM data, full vector data are used in the AMPERE data processing and inversions: the examples illustrate the vast increase in data density achieved by AMPERE. The spherical harmonic fit uses a longitude order of 5 and a latitude order of 20 in the range of colatitudes $0° \le \theta \le 60°$ [*Anderson et al*., 2014], and Figure 16.2 shows that under standard rate sampling, the data are sufficient to resolve signals with scales of ~1.5° in latitude [*Anderson et al*., 2017].

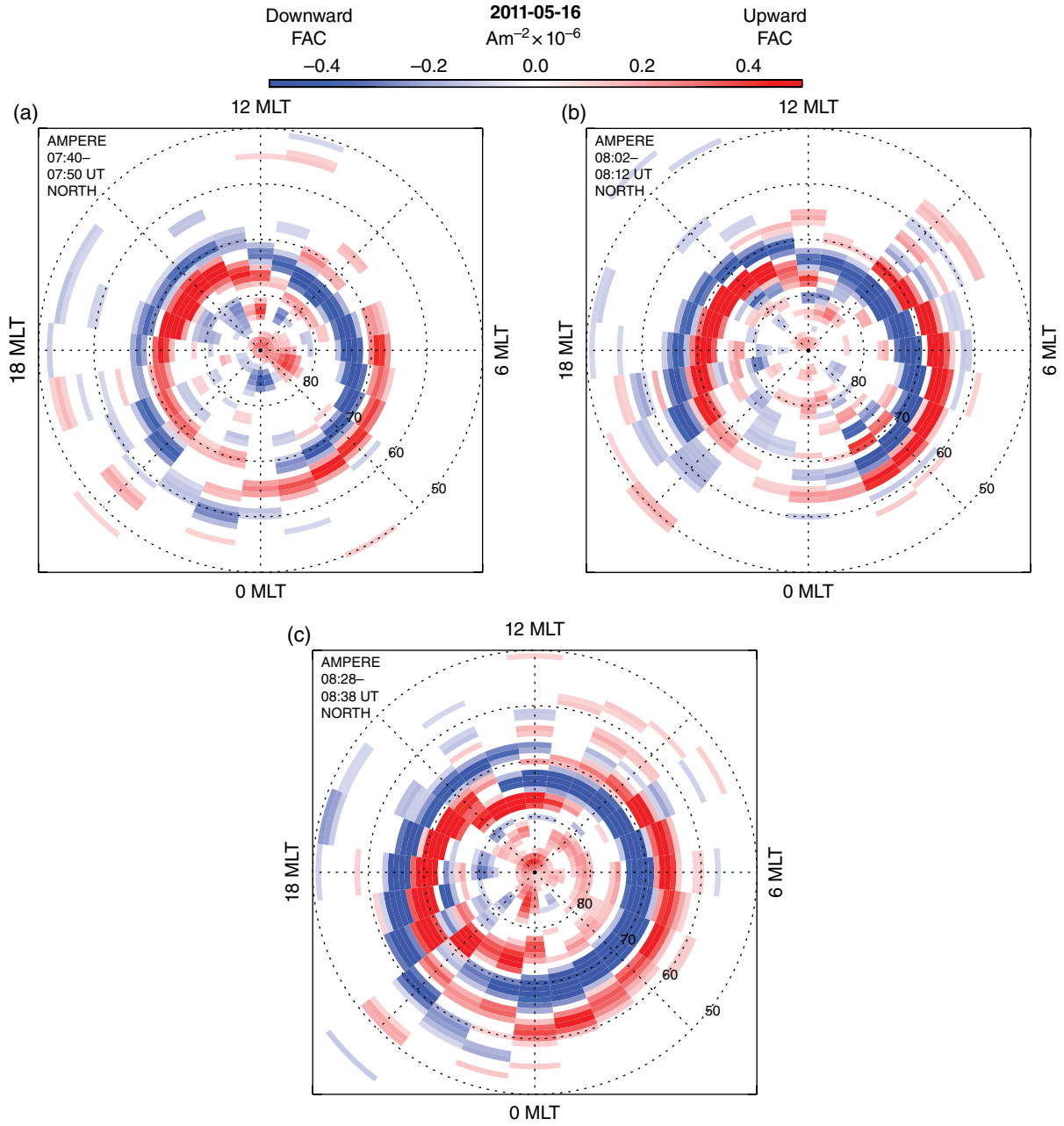

Figure 16.1 AMPERE current densities from (a) 07:45 UT, (b) 08:07 UT, and (c) 08:33 UT, 16 May 2011 in the Northern Hemisphere. The densities are plotted in polar coordinates with noon at the top of the page; dotted lines represent a grid of 3 hr MLT and 10° latitude, respectively. Upward current is defined as positive, with the color scale at the top indicating the densities in each panel. The panels show the progression of a substorm. From *Murphy et al.* [2013].

It is important to note that the TLM data were incapable of properly resolving magnetospheric reconfigurations or dynamics because at least 1 hr of data had to be accumulated to derive even a crude estimate of the currents. Only with the availability of AMPERE data was it possible to derive new global estimates of the Birkeland currents on 10 min timescales, shorter than a nominal magnetosphere-ionosphere reconfiguration time. With this advance, it finally became possible to observe the global dynamics of the Birkeland currents and truly resolve spatial and temporal dynamics. This review covers studies using both the Iridium-TLM and AMPERE data and the type of data used by each study are distinguished by the notations TLM or AMPERE data.

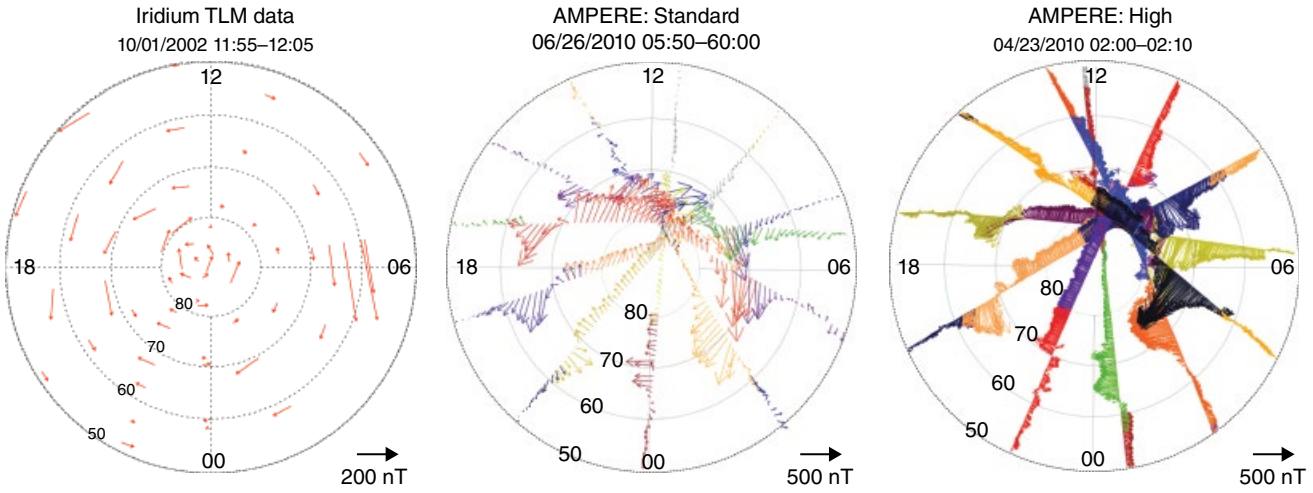

Figure 16.2 Comparison of magnetic field data returned from the Iridium Communications constellation of satellites in 10 min intervals with the engineering telemetry data (Iridium TLM) on the left and after the AMPERE development for standard or low rate (19.44 s between samples) and high rate (2.16 s between samples). All panels show reduced data from which the background field has been subtracted and further baseline removal has been applied. The magnetic perturbations are plotted as arrows originating at the point of measurement in the local horizontal plane and projected into AACGM latitude and local time. Arrow length scaling is shown by reference arrows at the lower right of each panel. For AMPERE data, different colors denote data from different satellites. For an example of the current densities derived from the magnetic data, see Figure 16.3.

While the Iridium TLM data were useful only for characterizing the large-scale average configuration of the Birkeland currents [*Anderson et al.*, 2000], the increased data rate achieved by AMPERE allowed studies of relatively small-scale features, which were previously only detectable with spacecraft constellations as Cluster [*Dunlop et al.*, Chapter 4, this volume] and Swarm [*Ritter and Lühr*, 2006]. With the global distribution of the AMPERE data, it became possible to identify the dynamics in the magnitudes of both R1 and R2 current, as well as the shape and distribution of the R1 and R2 current ovals and a method to do this algorithmically is described in *Clausen et al.* [2012] and *Coxon et al.* [2014a]. This review will focus on research conducted into Birkeland currents using the Iridium TLM and AMPERE datasets. Reviews of the current systems affecting Earth, and of magnetosphere-ionosphere coupling have previously been conducted [*Cowley*, 2000; *Milan et al.*, 2017], as have reviews of the different current systems [*Ganushkina et al.*, 2015, as well as the reviews found throughout this volume such as *Khurana and Liu*, Chapter 2, this volume].

The magnetic field data returned by AMPERE are fit to a continuous spherical harmonic fit and the curl of this fit is used to derive the radial current density making use of Ampère's law. Since it is the radial current density that is derived, equating this with the Birkeland current density is equivalent to assuming that the Birkeland current (and therefore the magnetic field) is radial. Due to the spacing of the satellites in each orbital plane, data are composed of a series of 10 min windows, evaluated every 2 min, and the data are on a grid of resolution 1° latitude and 1 hr of MLT. The data are presented in altitude adjusted geomagnetic (AAGCM) coordinates at an altitude of 780 km. We note that for ease of description, we adopt a convention in which the temporal midpoint of the 10 min window is used to describe an interval of data (such that an interval of data between 19:42 and 19:52 UT would be described as occurring at 19:47 UT).

16.3. REGIONS 1 AND 2 BIRKELAND CURRENT DURING GEOMAGNETIC STORMS

The first scientific study to use data from the Iridium spacecraft examined two geomagnetic storms, one on 22–23 September 1999 and the other on 21–22 October 1999 [*Anderson et al.*, 2002], Subsequent studies of Birkeland currents being driven by the solar wind have included case studies of geomagnetic storms from 2000–2015 using Iridium TLM data [*Anderson and Korth*, 2007; *Anderson et al.*, 2005; *Brandt et al.*, 2004; *Eriksson et al.*, 2008; *Liou et al.*, 2005; *Sitnov et al.*, 2010; *Stephens et al.*, 2013] and AMPERE data [*Knipp et al.*, 2014; *Le et al.*, 2016; *Lu et al.*, 2014; *Lyons et al.*, 2016; *Matsui et al.*, 2016; *Wilder et al.*, 2012] as well as case studies specifically of the dynamical evolution of the currents at activity onsets [*Anderson et al.*, 2014] or in conjunction with MMS observations in the magnetopause [*Anderson et al.*, 2016; *Le et al.*, 2016; *Matsui et al.*, 2016].

Maps of the currents during different IMF conditions have enhanced our knowledge of how the IMF changes Birkeland current patterns, as demonstrated by Figure 16.3. The ability to automatically detect the magnitude and location of the R1 and R2 currents [*Clausen et al.*, 2012; *Coxon et al.*, 2014a] has enabled statistical studies that confirm the magnitude of the Birkeland currents is consistent with driving by magnetic reconnection [*Coxon et al.*, 2014a,b] and the location of the Birkeland current ovals are consistent with expansions and contractions of the polar cap [*Anderson et al.*, 2014; *Clausen et al.*, 2012; *Coxon et al.*, 2014a,b]. Work has also shown that more R1 and R2 current flows when the current ovals are expanded during periods of dayside reconnection [*Anderson et al.*, 2014; *Coxon et al.*, 2014b], whereas Steady Magnetospheric Convection (SMC) events do not cause an expansion of the current ovals, but do cause more current to flow in the R1/R2 system [*Stephens et al.*, 2013]. Expansions of the current ovals observed with AMPERE are beginning to be used to identify periods of dayside reconnection [e.g., *Anderson et al.*, 2016], providing a new tool for identifying periods of driving. A more detailed review of the work that has been done on these topics follows in the rest of this section.

There is much to be done using AMPERE data to characterize and understand the Birkeland currents and their reaction to solar wind driving. Iridium TLM data have shown that the current ovals are in fact somewhat displaced toward dusk [*Anderson et al.*, 2005], although this has not yet been studied with AMPERE data. Comparisons of the aurora with Birkeland currents have been performed with Iridium TLM data [*Korth et al.*, 2004a] and AMPERE [*Carter et al.*, 2016; *Korth et al.*, 2014], although there is disagreement on whether upward current is colocated with auroral displays on the dusk flank of the polar cap, and the exact nature of the link between aurora and Birkeland current is still very much an open question. It has been suggested that the Birkeland current system can hold only a limited amount of current, and Iridium TLM data have been presented to support the idea that R1 current saturates during geomagnetic storms [*Anderson and Korth*, 2007], but more work needs to be done to substantiate this discovery. Work has demonstrated that the upward and downward currents in the Northern Hemisphere appear to be systematically stronger than those in the Southern Hemisphere [*Coxon et al.*, 2016a], and the nature of the physics underpinning this observation is also an open question.

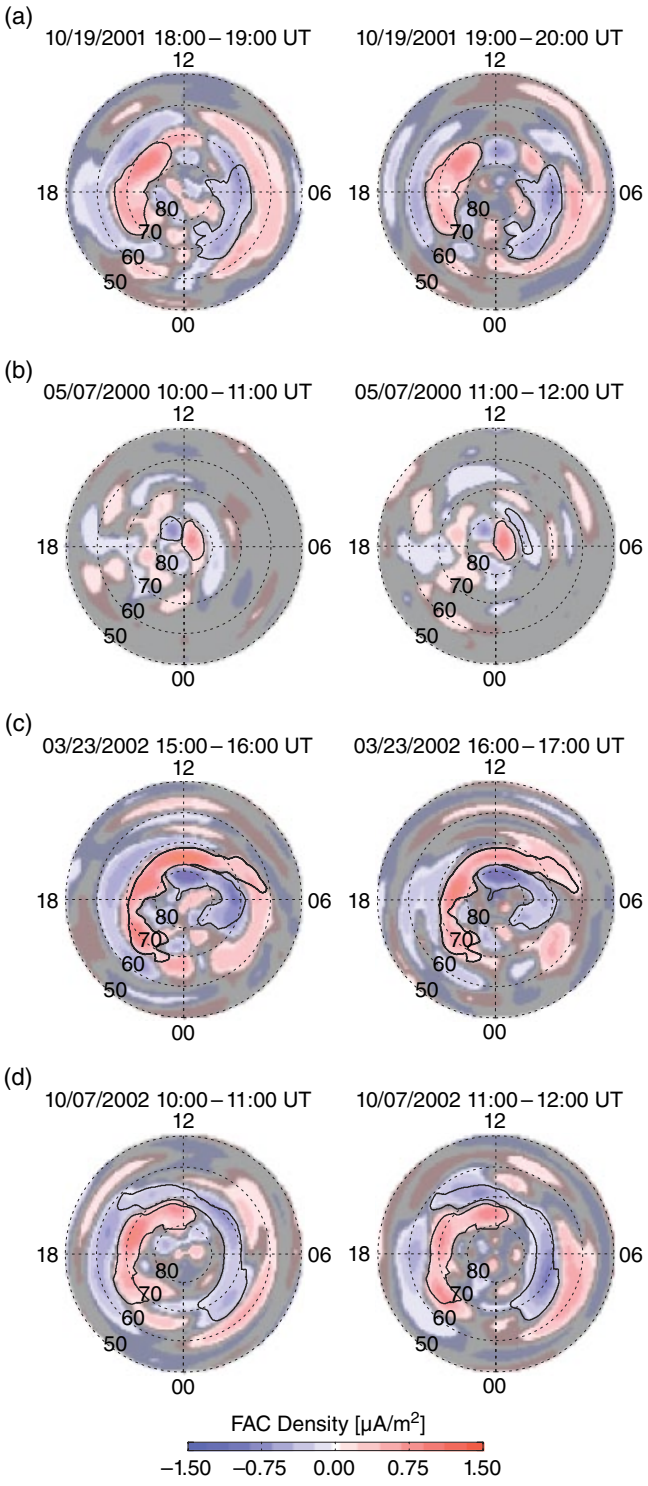

Figure 16.3 A plot showing examples of (a) southward, (b) northward, (c) dawnward, and (d) duskward IMF in current maps using Iridium TLM data. Upward currents are shown in red; downward currents are in blue; and grey shading indicates currents below the 2σ confidence level. Contours in the plots show the areas that stay constant between the time intervals plotted (above the 2σ confidence level). From *Anderson et al.* [2008].

16.3.1. Location

Looking at the global distribution of the currents is one of the key abilities of AMPERE that cannot be achieved via other methods. During southward IMF,

Birkeland currents are expected to be distributed in the Regions 1 and 2 (R1 and R2) current systems, and indeed this has been observed statistically with Iridium data [*Anderson et al.*, 2008] and subsequently AMPERE [*Carter et al.*, 2016]. Empirical Orthogonal Function (EOF) analysis and Principal Component Analysis (PCA) have been used to decompose AMPERE data into eigenfunctions that describe the modes of variability of the dataset; the first 12 eigenfunctions found by PCA are shown in Figure 16.4 [*Milan et al.*, 2015]. These eigenfunctions can be multiplied by scaling factors and combined to reconstruct maps of the current density (in this sense they are similar to spherical harmonics), and the single eigenfunction that describes the most variability in the dataset (called the primary component) is the R1 and R2 current system, with other components accounting for <10% [*Milan et al.*, 2015]. The first observations of the R1 and R2 current systems showed that they had, on average, a spiral structure with overlapping currents near noon [*Iijima and Potemra*, 1978]; this structure has been shown during intervals in which there is a nonzero B_Y component in the IMF and is seen in Figure 16.3c,d [*Anderson et al.*, 2008].

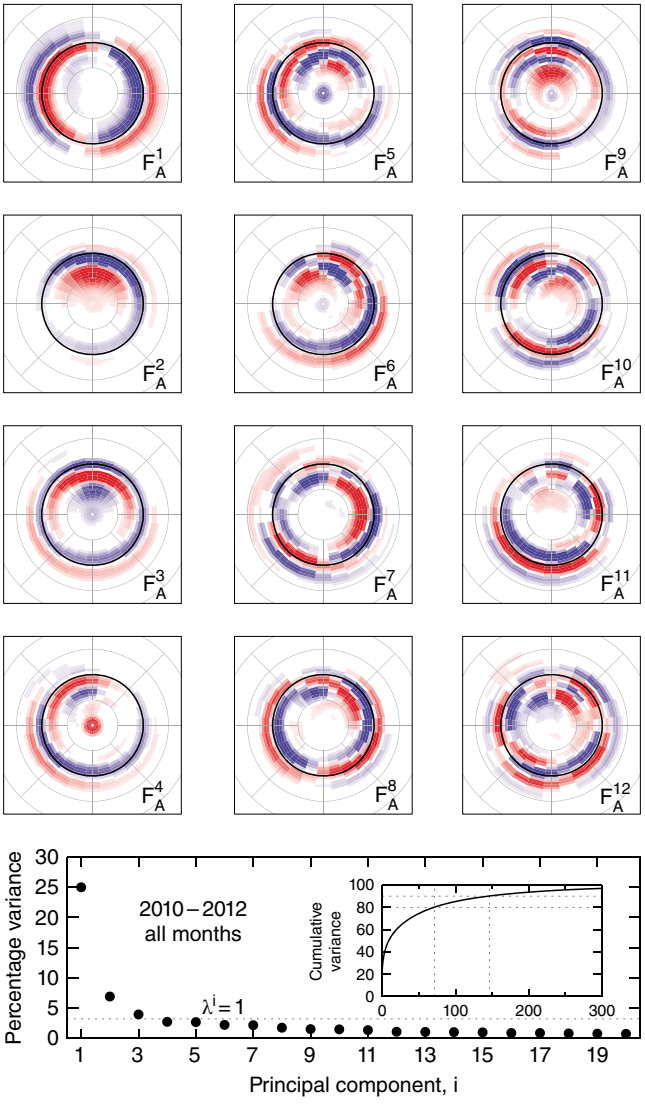

Figure 16.4 The 12 eigenfunctions responsible for the most variability in AMPERE data. F_A^1 shows the R1/R2 current system and is responsible for 25% of the variability in a current map, F_A^2 and F_A^3 are responsible for < 10% of the variability each, and the other eigenfunctions are responsible for < 1% each. There is no obvious candidate for the SCW in any of the eigenfunctions. From *Milan et al.* [2015].

The latitude of the equatorward edges of the R1 and R2 current ovals have been shown to be anticorrelated with *Kp* ($R = -0.68$), such that during periods of higher *Kp*, or during periods of southward IMF, the current ovals are observed to move to lower latitudes [*Anderson et al.*, 2002]. The location of the Birkeland currents in AMPERE data was also observed to be consistent with the evolution of SYM-H during six storms examined by *Zou et al.* [2014], with the current ovals moving between 5° and 10° equatorward during the geomagnetic storm. A storm on 17 April 2002 evaluated using Iridium data showed that the Birkeland currents moved 5° equatorward during the initial phase of the storm and then moved a further 5°–6° in the main phase [*Liou et al.*, 2005]. During the St. Patrick's Day storm in 2013, the R1 and R2 system was observed as southward IMF began and then expanded equatorward by ~1°–2° during a second interval of southward IMF; another expansion of ~2°–3° was observed during a third period of southward IMF, alongside developing smaller-scale currents [*Lyons et al.*, 2016]. A case study of the 17 March 2015 geomagnetic storm revealed that a prolonged interval of southward IMF led to observations of Birkeland currents moving equatorward by ~8°, with the most equatorward currents occurring at the most southward IMF [*Le et al.*, 2016]. Modeling of a CIR-driven magnetic storm showed that the field-aligned currents reduced in density and contracted when tail currents dominated in the model run, whereas they increased in density and expanded when the partial ring current was dominant [*Sitnov et al.*, 2010].

For comparison, the current ovals are also observed to expand during the growth phase of a substorm, prior to the onset of the expansion phase; this can be seen in Figure 16.1a,b, which shows the R1 and R2 currents moving 2°–3° to lower latitudes prior to the expansion phase onset [*Murphy et al.*, 2013]; this was corroborated by *Coxon et al.* [2014b], who employed a superposed epoch analysis to show that the average latitude of the current ovals moved toward the equator by 1°–2° over the 2 hr before substorm expansion phase onset. Although these increases in the size of the current ovals lie close to the threshold of AMPERE's ability to resolve latitudinal

features, they are consistent with increases observed in the latitude of the auroral ovals prior to expansion phase onset [e.g., *Milan et al*., 2009]. In contrast, steady magnetospheric convection (SMC) events do not result in significant equatorward expansion of the R1 current system, but the R2 current system does thicken, extending farther equatorward [*Stephens et al*., 2013], which suggests that the polar cap is not expanding in size but that the amount of current flowing increases.

The currents have been shown statistically to move to lower latitudes during periods of southward IMF [*Anderson et al*., 2008; Matsuo *et al*., 2015] and also during periods of enhanced solar wind electric field [*Korth et al*., 2010], which is consistent with magnetic flux being opened at the magnetopause by dayside reconnection. In Figure 16.3, the currents in the example of southward IMF are farther equatorward than in any other IMF condition. EOF analysis of AMPERE data showed that the function that explained the second most variability in the AMPERE dataset was associated with movement of R1 and R2 currents, but was only weakly correlated with solar wind driving [*Cousins et al*., 2015a]; however, contractions of the polar cap are not expected to be driven by the solar wind, which may explain why the correlation was not high. A substorm growth phase magnetic field model [*Yue et al*., 2015] was developed using empirical plasma sheet pressures from Geotail and THEMIS. Comparison with AMPERE showed a relatively poor correspondence, with the simulation only yielding downward currents in a very small part of the ionosphere relative to observations; however, the general pattern of the simulation results, if enlarged, did resemble the AMPERE observations. The model showed the equatorward motion of the auroras in the growth phase. Superposed epoch analyses show that the R1 current oval expands through the growth phase of a substorm and reaches maximum size ~ 15 min after expansion phase onset, before beginning to contract again [*Clausen et al*., 2012, 2013a,b; *Coxon et al*., 2014b]. This observation was interpreted as evidence for the current ovals expanding with dominant dayside reconnection and contracting with dominant nightside reconnection, as part of the expanding/contracting polar cap (ECPC) paradigm [*Cowley and Lockwood*, 1992; *Milan et al*., 2015; *Siscoe and Huang*, 1985]. The other results reviewed here also appear to be consistent with the ECPC model.

Expansions and contractions of the current ovals during geomagnetic storms are sometimes accompanied by a dawn-dusk asymmetry in the currents, which is also observed during storms. The geomagnetic storm of 1 October 2002 was found to show good agreement in R2 current between modeled currents and Iridium measurements [*Brandt et al*., 2004], and *Anderson et al*. [2005] presented an analysis of this storm and the subsequent storm, with minimum Dst = −163 nT. As the storm progressed, the Birkeland currents developed a dawn-dusk asymmetry during the main phase, with the currents lying at more equatorial latitudes on the dusk flank of the polar cap than on the dawn flank. During the recovery phase, the currents on both sides returned to approximately equal latitudes; a similar phenomenon was seen in a storm on 11–12 August 2000 [*Anderson and Korth*, 2007].

A statistical survey of geomagnetic storms found that the dusk currents were shifted equatorward, relative to the dawn currents, by an average of 2.4°, but that the extent to which the currents were asymmetrical was controlled in part by B_Y; dawn currents could be equatorward of dusk currents at large enough values of B_Y [*Anderson et al*., 2005]. B_Y is known to have a significant effect on the morphology of the Birkeland currents observed by AMPERE [*Carter et al*., 2016], with observations that there is a ~1.25 hr delay between a pulse of B_Y and a peak in dawnward current [*Wilder et al*., 2013] seemingly consistent with currents flowing as a result of forces acting to restore symmetry in cases of asymmetrical field lines [*Reistad et al*., 2016; *Tenfjord et al*., 2015], although results indicate that this effect is stronger in the summer hemisphere [*Green et al*., 2009]. Removing the effect of B_Y to look at the dawn-dusk asymmetry during geomagnetic storms confirmed that larger asymmetries occurred during the storm main phase; for each 100 nT in ASY-H, the dusk currents strengthened and moved approximately 1° equatorward relative to those on the dawn flank, attributed to ion pressure associated with the partial ring current [*Anderson et al*., 2005].

The knowledge that the current ovals observed by AMPERE expand and contract consistent with the ECPC has led to the data being used to verify periods of dayside (and nightside) magnetic reconnection. *Anderson et al*. [2016] used observations of the expanding R1 oval to show that dayside reconnection was occurring and thus demonstrated that MMS observations of a deviation in magnetopause location was consistent with magnetopause erosion due to dayside reconnection. Expansions of the current ovals were also used to identify dayside reconnection intervals in an investigation of GPS scintillations by *Clausen et al*. [2016].

Field-aligned currents facilitate the travel of particles from elsewhere in the magnetosphere into the ionosphere, and are therefore intimately related to auroral displays. Currents tend to be stronger when the current ovals are expanded [*Coxon et al*., 2014b], consistent with the dynamic behavior of emissions previously established by global auroral imaging using such missions as IMAGE and Polar. Upward Birkeland currents are thought to be colocated with auroral precipitation [*Waters et al*., 2001]; however, recent results differ on whether upward current on the dusk side of the polar cap are well colocated with

aurora in this region [*Carter et al*., 2016; *Korth et al*., 2014]. This is an open question that needs to be resolved in future studies using AMPERE (and perhaps other Birkeland current measurements) in conjunction with auroral observations.

16.3.2. Integrated Total Current

As well as enabling hitherto unprecedented views of the location of the currents flowing in the magnetosphere, AMPERE provides for analysis of the total amount of current flowing, both by using current density and by calculating the magnitude of the current flowing [e.g., *Anderson et al*., 2014]. Some studies have created indices that describe the maximum magnetic perturbations detected by Iridium spacecraft, and found that these measures of current activity were correlated with the AE index calculated using ground magnetometers, indicating that the magnetic perturbations and consequently the Birkeland currents increased with geomagnetic activity [*Anderson et al*., 2002] and after the commencement of geomagnetic storms [*Liou et al*., 2005]. This has been substantiated by AMPERE, which shows that more current flows in the R1 and R2 current systems at times of more southward IMF [*Anderson et al*., 2014; *Cousins et al*., 2015a; *Matsuo et al*., 2015], with current density increasing as the current ovals move to equatorward latitudes in the geomagnetic storm of 17 March 2015 [*Le et al*., 2016]. Superposed epoch analyses also appear to show that the current magnitudes peak approximately coincident with the current oval reaching its equatormost point [*Coxon et al*., 2014b].

Steady magnetospheric convection (SMC) events have been found to increase the density and thickness of the R1 and R2 current systems [*Stephens et al*., 2013], and the solar wind electric field is the most important factor driving Birkeland current intensities during southward IMF [*Korth et al*., 2010], which suggests that the currents are driven by magnetic reconnection, especially at the magnetopause. Indeed, it has recently been explicitly demonstrated that R1 and R2 current magnitudes are consistent with driving by both dayside and nightside reconnection [*Coxon et al*., 2014a,b; *Milan et al*., 2015]. Furthermore, examination of upward and downward Birkeland current flowing as a function of both reconnection and conductivity shows that the amount of current (averaged over 27 days to remove solar effects) is well represented by a combination of conductivity enhancements due to solar illumination and driving by dayside reconnection [*Coxon et al*., 2016a]. In the same paper, the magnitudes of the upward and downward current in the Northern Hemisphere were systematically larger than the Southern Hemisphere even when seasonal and diurnal effects were taken into consideration, implying that an asymmetry might be present in the Birkeland currents in each hemisphere. Although the confluence of the orbital tracks of the Iridium constellation lies farther from the pole in the Southern Hemisphere than in the Northern Hemisphere, this asymmetry seems likely to be a physical phenomenon, since observations show that there are differences in ionospheric convection [*Förster and Haaland*, 2015] associated with asymmetries in Earth's magnetic field [*Cnossen and Förster*, 2016; *Laundal et al*., 2016], so it is reasonable that such an asymmetry may also be present in the Birkeland currents.

Estimates of the energy input to the ionosphere have also been made in two studies, which combined data from the Iridium constellation with data from SuperDARN to estimate the total electromagnetic energy contribution by calculating the Poynting flux [*Korth et al*., 2008a; *Waters et al*., 2004]. In the first study, the total energy input during the event was estimated to be 50 GW and the Iridium and SuperDARN estimate showed good agreement with Defense Meteorological Satellite Program (DMSP) calculations of Poynting flux [*Waters et al*., 2004]. In the second study, the Iridium and SuperDARN calculation was corrected for a perceived underestimate compared to the DMSP calculation, and the total energy input was estimated at 188 GW, which was found to be an order of magnitude greater than the 20 GW from particle precipitation calculated using auroral imaging [*Korth et al*., 2008a].

Two geomagnetic storms during 10–13 August 2000 were found to exhibit evidence for R1 current saturation, a phenomenon in which magnetic perturbations associated with R1 current act to reduce the subsolar magnetic field and therefore also reconnection rate [*Anderson and Korth*, 2007, and references therein]. The second storm in this period showed a maximum interplanetary electric field E_Y, which was 3.6 times greater than that of the first storm, but the Birkeland currents in the second storm were only twice as big. A sample of 23 events was used to fit a power law of current $I = 4.2 + 2.6E_Y^{0.48}$, indicating that the currents do indeed show the theorized saturation. However, no margins of error were calculated and the conclusion mostly comes from a small number of data at $E_Y > 10\,\mathrm{mV\,m^{-1}}$. Similar analyses have not yet been performed with AMPERE data to establish whether the currents do saturate.

16.4. THE SUBSTORM CURRENT WEDGE

Substorms are a key mechanism driving nightside Birkeland currents, and AMPERE enables, for the first time, snapshots in which the current density is visible across the entire substorm current wedge (SCW) region [*Clauer and McPherron*, 1974; *McPherron et al*., 1973]. As a result, much work has been done using AMPERE to examine the SCW, including several case studies of

substorms [*Connors et al*., 2014, 2015; *Murphy et al*., 2012, 2013; *Sergeev et al*., 2014a]. Other studies have used a statistical approach [*Clausen et al*., 2012, 2013a,b; *Coxon et al*., 2014b, 2017]. It has been found that the onset of nightside currents, presumably reflecting onset of return convection in the magnetotail, is critical to the development of the global R1/R2 current system [*Anderson et al*., 2014]. While most authors agree that Birkeland currents on the nightside are intimately related to substorms, the exact nature of the SCW is one of the biggest open questions in the field, and studies using AMPERE are critical to developing our understanding of substorms. The traditional picture of the SCW involves a single current flowing into the ionosphere on the post-midnight side and a single current flowing out of the ionosphere on the premidnight side, in the same sense as R1 [*Clauer and McPherron*, 1974]. There is debate as to whether this picture is accurate, or whether there is also a current in the sense of R2, which flows as a result of a substorm as part of a "two loop" substorm current wedge [*Sergeev et al*., 2011, 2014b]. Another topic of debate is whether the currents that compose the SCW should be considered as R1 and R2 currents, or whether they should be considered as distinct currents that happen to flow in a similar sense. To differentiate between the models of *Clauer and McPherron* [1974] and *Sergeev et al*. [2014a], we refer to them as "single loop" and "two loop" current wedges in the rest of this section while reviewing the work to date in more detail.

Although the large-scale structure of the SCW is an open question that is perfect for AMPERE, the SCW is also thought to have small-scale structure, which may be beyond the limitations of the AMPERE dataset. Authors have used Cluster data to show that the SCW may comprise tens of filamentary current sheets, rather than broad regions of current [*Forsyth et al*., 2014] and MMS observations found current sheets with a thickness of 25 km in the plasma sheet during substorms [*Nakamura et al*., 2016]. As such, work with AMPERE focuses on large-scale structure.

Case studies have contributed evidence to this debate. *Murphy et al*. [2013] used AMPERE data from events in which the footprint of the Iridium satellite contributing to the AMPERE data was close to the onset of the substorms in question, identifying three events in 2010 and 2011 for which this was the case. Observations for two of the events showed R1 and R2 current flow, but such flow was flanked by additional current systems in both of those events (an example is shown in Fig. 16.1); the third event showed no sign of the R1 and R2 current system in the expected sense. Despite the structure observed in the cases chosen, they concluded that averaging latitudinally could replicate the single loop SCW of *Clauer and McPherron* [1974]. *Connors et al*. [2014] showed a case study of a substorm in AMPERE data, concluding that the two loop substorm current wedge was not supported by their observations. However, the AMPERE data they present appear to show an enhancement in R2-sense currents flowing equatorward of the R1-sense currents after expansion phase onset, consistent with the two loop model of *Sergeev et al*. [2011]; in subsequent analysis of the event, they noted that the substorm had involved regions both near Earth and farther down the magnetotail [*Connors et al*., 2015]. Finally, a case study employing AMPERE data in addition to four GOES spacecraft and three THEMIS spacecraft [*Sergeev et al*., 2014a] found that the current wedge more closely resembled the two loop substorm current wedge [*Sergeev et al*., 2014b]. As such, all the case studies done using AMPERE data appear to support the two loop SCW, rather than the single loop model.

A number of statistical analyses of substorm current development have also been performed. *Clausen et al*. [2013a,b] examined substorm expansion phase onsets in the first four months of 2010, looking first at the morphology of the currents during substorms [*Clausen et al*., 2013a]. The authors found that the R1 current density on the nightside was enhanced after substorm expansion phase, and that R1 currents were dominant on the dayside prior to onset and on the nightside after onset. They found no corresponding enhancement in R2 current, concluding that the currents were in agreement with the single loop SCW [*Clauer and McPherron*, 1974]. Although these statistical studies have not shown any evidence of the two loop SCW, it should be noted that they did not rotate or scale the current maps from AMPERE with the latitude or MLT of substorm onset, which might have allowed some spatial smoothing to occur.

Clausen et al. [2013b] then turned to examining the influence of the amount of open magnetic flux on the substorms observed, concluding that when more the magnetosphere contained more open magnetic flux at the time of substorm onset, the substorm was more intense, presenting evidence that the R1 current density (among other parameters) was more enhanced during substorms occurring at times of higher magnetic flux. Another superposed epoch analysis was performed by *Coxon et al*. [2014b], who examined AMPERE data for 3 yr between 2010–2012, looking at the size of the R1 and R2 current ovals and the R1 and R2 current magnitudes. As well as finding that the R1 and R2 current ovals increased in size until ~10 min after substorm onset, they also found that R1 and R2 current were both enhanced after onset and that the ratio of R1 current to R2 current increased after substorm onset. They concluded that the auroral electrojet at the ionospheric footprint of the SCW

was closing R1 current in the dawn flank through the R1 current system on the dusk flank of the polar cap, but that R2 current was also enhanced, providing insight into the larger structure of the SCW [*Coxon et al*., 2014b]. A follow-up study of the morphology of the current systems (2010–2015) showed that if the substorms were rotated to the MLT of substorm onset and binned by substorm onset latitude, the R1 and R2 current systems both showed enhancement at substorm onset [*Coxon et al*., 2017], consistent with the two loop SCW [*Sergeev et al*., 2014a]. The 12 eigenfunctions that describe the most variability in the AMPERE dataset (Fig. 16.4) were found by principal component analysis [*Milan et al*., 2015], but none of these eigenfunctions appear to be associated with the SCW and *Milan et al*. [2015] concluded that there was no eigenfunction representing the SCW. The fact that the SCW can be well described in terms of R1/R2 sense currents gives an insight as to why no such eigenfunction was found.

Murphy et al. [2012] investigated a somewhat different aspect of Birkeland current variation during substorms, investigating the phenomenon of auroral dimming first observed by *Pellinen and Heikkila* [1978]. They found evidence for auroral dimming in a substorm that was located under the track of an Iridium satellite, noting that the upward Birkeland current density in the MLT of substorm onset reduced close to the latitude of substorm onset consistent with observations of a decrease in auroral intensity prior to onset. This was expanded upon by *Coxon et al*. [2017], who found that a superposed epoch analysis of current density close to the location of substorm onset showed a similar decrease in density prior to substorm onset.

In summary, the recent history of the substorm current wedge is one of an ever more complex system. Authors have observed smaller-scale structures within the traditional, large-scale substorm current wedge [*Murphy et al*., 2013; *Nakamura et al*., 2016] and more complicated large-scale structures have been proposed [*Sergeev et al*., 2011, 2014b]. Although AMPERE has shed significant light on the behavior of the Birkeland currents around substorm expansion phase onset, results have been interpreted differently by different authors. Case studies appear to demonstrate the existence of a two loop current system, and despite statistical studies which do not concur, the most recent statistical study is consistent with this view [*Coxon et al*., 2017]. The exact morphology of the currents close to substorm onset, and the behaviour of currents prior to onset, remain open questions.

16.5. OTHER CURRENT SYSTEMS

While we have reviewed the largest Birkeland current systems (sections 16.3 and 16.4), it is also important to review the work that has been done with AMPERE on current systems outside of these. One of these current systems is the banana current system, which is driven by pressure gradients in the magnetosphere and flows eastward on the earthward side of a peak in pressure located within the inner magnetosphere [*Liemohn et al*., 2013]. Consequently, a westward current is required to close it, either through the ionosphere (path 1) or through a current on the far side of the same pressure peak in the inner magnetosphere (path 2). *Liemohn et al.* [2013] concluded that the current would close in the magnetosphere rather than in the ionosphere, and the resulting shape gave rise to its moniker. Observations with AMPERE showed no sign of a pair of upward and downward Birkeland currents of the required sense for path 1 at low latitudes [*Stephens et al*., 2016], which is consistent with the original conclusion that the current closed through path 2 [*Liemohn et al*., 2013].

Observations of an auroral arc made before a substorm showed that the arc was located ~4° equatorward of the R1/R2 interface in the early growth phase but this decreased to ~1° shortly before onset [*Motoba et al*., 2015]. AMPERE data were used to infer the location of the R1/R2 boundary, and RBSP-B data when the spacecraft was very close to the arc showed that the arc was connected to the magnetotail by an upward Birkeland current on the tailward side of an enhancement in plasma pressure, which was interpreted as evidence for localized pressure gradients driving Birkeland current and therefore the auroral arc [*Motoba et al*., 2015].

Another current system beyond the structures of Regions 1 and 2 current and the SCW has been observed by AMPERE. During intervals of northward IMF, the R1 and R2 current systems are weakened, and a different dominant current system is observed; this system is called NBZ (because it occurs coincident with northward B_Z). Periods of northward IMF both before and during the recovery phase of geomagnetic storms have resulted in current distributions in AMPERE consistent with the expected NBZ current system [*Eriksson et al*., 2008; *Le et al*., 2016] and statistical analysis of Iridium current density also shows these distributions when binned by IMF conditions [*Anderson et al*., 2008]. Birkeland current densities higher than $0.7\,\mathrm{mA\,m^{-2}}$ and solar wind proton densities lower than $4\,\mathrm{cm^3}$ are associated with the occurrence of high-latitude dayside aurora [*Korth et al*., 2004a], and the motions of upward currents within an NBZ current system on 15 May 2005 were linked to the motion of a transpolar arc in the same geomagnetic storm [*Eriksson et al*., 2008]. Averaged Iridium TLM data suggest that the NBZ current system does not occur in the winter hemisphere and that Birkeland current is reconfigured to the nightside in the winter hemisphere, in comparison to the summer hemisphere [*Green et al*., 2009]. Periods of sustained northward IMF allow for the identification of currents driven by a viscous

Kelvin-Helmholtz interaction, and such an interaction is thought to account for <0.2 MA [*Korth et al*., 2005].

16.6. CONDUCTIVITY AND ITS EFFECT ON BIRKELAND CURRENTS

Conductivity is a relatively underrepresented topic for AMPERE studies so far. The large spatial scale afforded by AMPERE data seemingly makes AMPERE a natural choice for any large-scale study of conductivity, or such phenomena as Joule heating, but not many authors have used AMPERE data to tackle these open questions. Two of the main studies to examine the issue used Iridium TLM data, with one study comparing estimates of Birkeland currents using SuperDARN and conductivity estimates to data [*Green et al*., 2006] and another directly estimating the conductivity from Iridium TLM data [*Green et al*., 2007]. *Coxon et al*. [2016a] used a model with dayside reconnection and conductivity inputs [*Milan*, 2013] to compare the monthly averaged modeled Birkeland currents to monthly averaged AMPERE observations, finding good agreement between modeled results and AMPERE, but a distinct asymmetry between the current flowing in the Northern and Southern Hemispheres.

Ionospheric vorticity has been used as a proxy for Birkeland current flow, which has been shown to be a reasonable proxy in an average sense [e.g., *Chisham et al*., 2009], although variations in conductivity lead to disagreements between the vorticity and the actual currents. Some authors have combined radar data with models of ionospheric conductivity to estimate the Birkeland currents directly, and these estimates have been compared with Iridium TLM data; this technique does well in sunlit conditions where SuperDARN covers the area of interest, but poorly on Earth's nightside and where SuperDARN data were not available [*Green et al*., 2006]. This is consistent with underestimates of Birkeland currents from the Lyon-Fedder-Mobarry magnetohydrodynamic model on the nightside [*Korth et al*., 2004b], and *Green et al*. [2006] suggested that estimates of conductivity due to particle precipitation were to blame. A technique to estimate the conductivity from Iridium TLM data showed enhanced conductivity between the R1 and R2 current systems and estimated the ratio between Hall and Pedersen conductivity at close to unity [*Green et al*., 2007].

The Birkeland currents determine the curl-free component of the height-integrated horizontal current in the ionosphere $J_{\perp,\,\mathrm{cf}}$. Fukushima's theorem states that, from the Earth's surface, the magnetic perturbations due to Birkeland current flow are canceled completely by the magnetic perturbations due to these curl-free currents, in the case where the magnetic field is radial and the conductivity is uniform [*Fukushima*, 1969, 1976], such that ground magnetic perturbations are directly associated only with the divergence-free component of the horizontal ionospheric current $J_{\perp,\,\mathrm{df}}$. *Laundal et al*. [2015] took advantage of the fact that the total horizontal current $J_{\perp}$ could be decomposed into $J_{\perp,\,\mathrm{cf}}$ and $J_{\perp,\,\mathrm{df}}$, and as a result argued that where $J_{\perp} = 0$, $J_{\perp,\,\mathrm{df}}$ will be entirely determined by $J_{\perp,\,\mathrm{cf}}$, such that the global Birkeland current distribution alone determines the local magnetic perturbation. This decomposition has proven useful in evaluating the relative contributions within the polar cap at different times of day, showing that during sunlit hours, the Hall current system dominates measurements made on the ground, whereas in darkness, the Birkeland current contribution can be measured using ground magnetometer data. This was attributed to conductivity in the polar cap approaching zero when the polar cap is in darkness [*Laundal et al*., 2015, 2016].

Birkeland currents themselves vary with conductivity, relying primarily on solar illumination on the dayside and particle precipitation at premidnight magnetic local times [*Laundal et al*., 2016]. It is possible to model the amount of Birkeland current flowing in the magnetosphere with a model that takes magnetic reconnection rates as input, combined with estimates of the ionospheric conductivity [*Milan*, 2013], which can in turn also be modeled using functions of the solar zenith angle [*Moen and Brekke*, 1993; *Robinson and Vondrak*, 1984]. Such a model has been constructed, and has been tested by using the dayside reconnection rate, averaged over a 27 day period. Then, the magnitudes of upward and downward current observed by AMPERE for each hemisphere can be calculated and summed, and the 27 day average of that quantity can be compared to the modeled current magnitudes [*Coxon et al*., 2016a], showing excellent agreement between such a model and observations. This is consistent with the view that Birkeland currents are driven by the convection of the magnetosphere. However, as mentioned in section 16.3.2, the amount of current flowing was found to be asymmetrical between the Northern and Southern Hemispheres [*Coxon et al*., 2016a]. The reasons for this remain open to question.

16.7. MODELING, ASSIMILATION, AND SIMULATION

Data from AMPERE have also been used to develop or test statistical models, as inputs to ionospheric electrodynamics assimilation, and in comparisons with physical simulations of the magnetosphere-ionosphere system. In this section, we will give an overview of the models that have been validated using AMPERE data, in order to demonstrate how useful this dataset is to those trying to model the electrodynamics of the ionosphere. The global distribution and continuous availability make these data

and products particularly amenable to assimilation analyses. In addition, because the Birkeland current density is conserved from low to high altitudes, and because the current is a fundamental quantity evaluated within MHD, as distinct from auroral emission for example, the AMPERE results have proven to be particularly useful for testing results from MHD magnetospheric simulations.

16.7.1. Model Development and Validation

Various model results have been validated using AMPERE data over the course of its availability, and AMPERE data have also been used as the underpinning for empirical models [*Yue et al*., 2015]. The first such comparison of AMPERE data to model results was conducted by *Papitashvili et al*. [2002], who constructed a model of the Birkeland current morphology with IMF direction and season using Ørsted and Magsat data. They found agreement with the results reviewed in section 16.3 and compared their model with Iridium TLM data, concluding that the two corresponded well. Subsequent work based on Iridium TLM data that decimated the intervals used for the statistics using only those for which the Birkeland current distributions were stable found that the southward and northward IMF distributions were much more distinct than were derived from statistical models using single satellite data that could not be as selective in the intervals included in the analysis [cf. *Anderson et al*., 2008; *Korth et al*., 2010].

The amount of open flux in the magnetosphere, also known as the magnetotail magnetic flux (MTF), can be modeled using spacecraft measurements of the magnetic field in the magnetotail in conjunction with solar wind measurements. This procedure has been performed using Cluster data in the magnetotail and solar wind data from OMNI to estimate the MTF in 2001 to 2009 using automated identifications of the different regions of the magnetotail [*Boakes et al*., 2014] and also in October 2010 using visual identifications [*Shukhtina et al*., 2016]. It would in principle be possible to extend this using more recent identifications of Cluster in the magnetotail lobes [*Coxon et al*., 2016b]. MTF estimates were compared to IMAGE data in August/September 2005 and AMPERE data in October 2010, achieving correlations of 0.7.

An Automated Forward Modeling (AFM) technique has been developed that allows for the total current and the location of the auroral electrojet to be output, using a nonlinear optimization algorithm (based on the Levenberg-Marquardt method) with a model of auroral current systems and taking ground magnetometer data as input [*Connors and Rostoker*, 2015; *Connors et al*., 2014, 2015]. This technique can be used globally (AGM), regionally (ARM), and meridionally (AMM). Results from the ARM technique indicated that three-dimensional current system parameters could be inferred from ground magnetometer data [*Connors et al*., 2014], and AMPERE was used to identify intervals at which an auroral electrojet should be visible such that AMM could be compared to the meridional ionospheric currents estimated using the Spherical Elementary Current Systems (SECS) technique [*Pulkkinen et al*., 2003], finding agreement within 10% [*Connors and Rostoker*, 2015]. The technique of gridded integration used by *Connors et al*. [2014] was used to identify the difference between the upward and downward field-aligned currents in each sector, which was inferred to be the meridional current; comparison of this AMPERE-derived quantity to the AMM technique showed reasonable (if unquantified) agreement between the two estimates [*Connors and Rostoker*, 2015].

16.7.2. Assimilation Studies

Assimilation analysis for ionospheric electrodynamics has an extensive history [*Knipp et al*., 1989; *Richmond and Kamide*, 1988] and AMPERE data have proven to be a particularly useful input to the Assimilative Mapping of Ionospheric Electrodynamics (AMIE) algorithm [*Lu*, 2016; *Matsuo et al*., 2015; *Wilder et al*., 2012]. The AMIE procedure can ingest various datasets in addition to AMPERE and can yield spatial patterns that are more distinct and that lack small-scale, rapidly oscillating features that can occur in the spherical harmonic fitting due to disparities in the latitude and longitude resolution of the input data [*Matsuo et al*., 2015]. The AMIE outputs relying solely on measurements taken from the ground grossly underestimate the cross-cap potential in comparison with satellite data [*Lu*, 2016; *Marsal et al*., 2012]. Figure 16.5 shows results from *Wilder et al*. [2012] using AMIE for the 5 April 2010 storm at 00:30 UT. The panel on the left shows the electromagnetic energy flux derived from ground magnetometer data together with SuperDARN flows and DMSP satellite data. The panel on the left is for the same interval but after adding the AMPERE data. The magnitude and the distribution of the energy flux are dramatically different between the two. AMIE has also been used with AMPERE to show that during the recovery phase of a geomagnetic storm, when the IMF was northward, intense Joule heating associated with NBZ currents took place in the dayside polar regions [*Wilder et al*., 2012]. Another method for assimilating satellite magnetic perturbations in estimating ionospheric properties is the Utah State University data assimilation model, which when using Iridium magnetic perturbations together with other measurements exhibits good agreement with SuperDARN returns [*Zhu et al*., 2012].

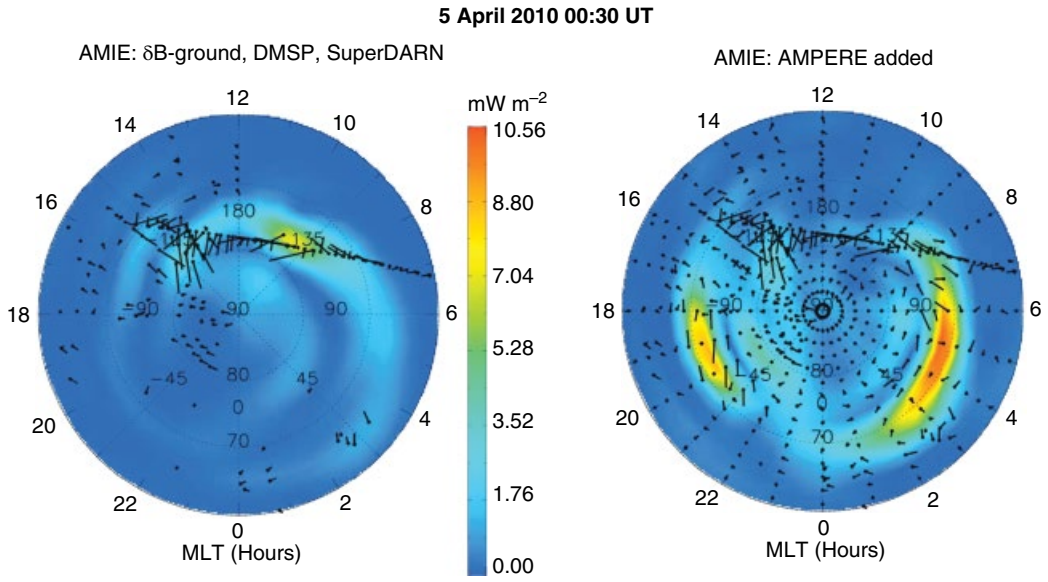

Figure 16.5 Results using AMIE of assimilative determination of ionospheric Joule heating derived for 00:30 UT on 5 April 2010 using ground magnetometer, SuperDARN, and DMSP data only (left) and when also using AMPERE results (right). The dramatic difference in distribution and intensity of the heating reflects the importance of including these additional data in such analysis. Adapted from *Wilder et al.* [2012].

Perhaps the most stringent test whether the electrodynamics using AMIE are valid is given by comparisons with storm-time thermospheric density dynamics. The AMIE procedure using AMPERE has been used as an input to the Thermosphere-Ionosphere (-Mesosphere)-Electrodynamics General Circulation Model, known as TI(M)EGCM. Initial results showed that TIEGCM was underestimating the induction currents in the Earth's surface, but improved the model's minimum timescale of variation from 6 hr to 10 min [*Marsal et al.*, 2012]; simulations of ground observations only improved modestly when the conductivities in the model were improved [*Marsal*, 2015]. Traveling atmospheric disturbances were modeled with TI(M)EGCM [*Lu et al.*, 2014], and comparison to data showed that neutral winds over the polar region were well reproduced. In addition, the densities at the GOCE and CHAMP satellites and those derived from the thermospheric simulation showed remarkably similar dynamics as shown in Figure 16.6 indicating that the assimilated electrodynamics closely reproduced the thermospheric response even though the model underestimated the neutral mass density and overestimated the storm recovery time somewhat [*Lu et al.*, 2014].

An even more ambitious assimilation challenge is to use data to adjust MHD simulations. An initial study of the feasibility was conducted by *Merkin et al.* [2016]. They found that rather than attempting to assimilate the currents, it was actually computationally more stable and hence more feasible to assimilate the low altitude magnetic perturbations as a boundary condition. By deriving the covariance matrix between the low altitude signals in the closed field region, attributed to R2 currents and the simulation, their initial analysis demonstrated that the technique could be used to reduce the discrepancy between the simulation and the observations. Future work to actually ingest the low altitude boundary into the simulation would require resolving potentially competing effects of the solar wind/IMF drivers for the simulation and the signals associated with the R1 currents. Given the close linkage between the R1 and R2 currents [cf. *Carter et al.*, 2016] allowing potentially conflicting drivers in the simulation assimilation scheme is a problem that has yet to be solved.

16.7.3. Simulation Comparisons

Magnetohydrodynamical models have been a subject of research in the community since the 1970s [e.g., *Merkin et al.*, 2016, and references therein], but for most of the history of the field, it has been difficult to compare their global predictions of Birkeland current to data. AMPERE allows for MHD modeling to be directly compared to global measurements of the Birkeland current systems. The Lyon-Fedder-Mobarry (LFM) model is an established MHD model, and has been well compared with Iridium and AMPERE data. High resolution simulations with this model generated R1 currents that exceeded results from the Iridium TLM derived field-aligned currents and that were attributed to underestimates in Iridium estimates of Birkeland current [*Korth*

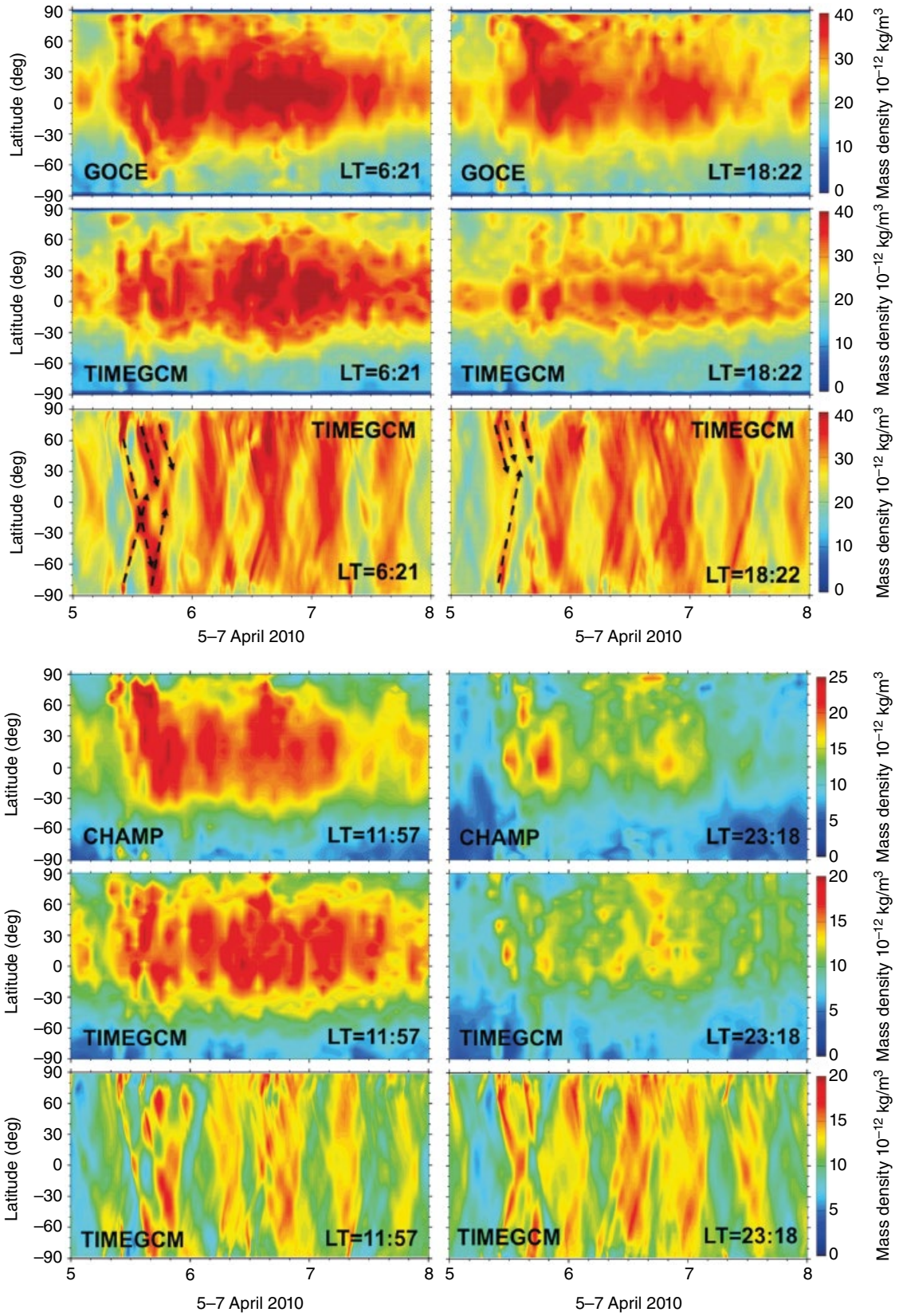

Figure 16.6 Thermospheric circulation results for the 5–7 April 2010 geomagnetic storm compared against neutral densities derived from accelerometer data from the GOCE and CHAMP satellites [*Lu et al.*, 2014]. Neutral density determinations from the GOCE and CHAMP satellites are shown in the top panels and reflect the elliptical orbits of the satellites. The neutral densities evaluated along the GOCE and CHAMP orbits from the thermosphere, ionosphere (mesosphere), exosphere, general circulation model, TI(M)EGCM, are shown in the middle panels. The TI(M)EGCM results were obtained using the AMIE procedure inputs for ionospheric electrodynamics using AMPERE data. Bottom panels show the neutral density at a fixed altitude clearly showing the traveling density disturbances between the polar regions. Adapted from *Lu et al.* [2014].

et al., 2004b, 2008b] and/or overestimates in the simulated electric field [*Korth et al*., 2008b]. In the same comparisons, the simulated R2 currents and nightside currents underestimated the observations, indicating that the simulation ionospheric conductivity on the nightside was too low [*Korth et al*., 2004b]. A similar problem was exhibited in the simulations run by *Korth et al*. [2008a], and both simulations underestimated the R2 current.

In further work, a case study of an event that demonstrated low R2 current and weak solar wind driving was conducted and the LFM model reproduced the currents derived from Iridium TLM data [*Merkin et al*., 2007]. Another case study performing comparisons with AMPERE results and a higher resolution run of the LFM model for the 3–5 August 2010 geomagnetic storm found that the simulated magnetic perturbations well reproduced AMPERE observations except for some peaks in current density that exceeded the AMPERE measurements. The simulation yields filamentary currents with longitudinal extent smaller than the spacing between Iridium orbit tracks the discrepancy was attributed to an underestimate in the AMPERE inversions [*Merkin et al*., 2013]. *Kleiber et al*. [2016] developed a framework to compare simulations to satellite products by automatically detecting R1 and R2 current regions and found that high-resolution simulations corresponded well to AMPERE observations in an example event.

A study of the Whole Heliosphere Interval (Carrington Rotation 2068) was conducted, in which the results of the LFM model were compared with AMPERE observations, both parameterized by eight IMF clock angles: this showed that the patterns agreed well, and that the ratio R1/R2 decreased as the resolution of the model increased [*Wiltberger et al*., 2016], suggesting that the low R2 currents shown in previous simulations [*Korth et al*., 2004b, 2008a] were due to underestimation of the R2 currents in the lower resolution simulations. A previous statistical study was conducted by *Korth et al*. [2011], comparing Iridium TLM results with the Space Weather Modeling Framework (SWMF) comprising a magnetosphere model coupled to the Rice Convection Model (RCM). This simulation showed that modeled currents and currents observed with AMPERE had a correlation of ~0.8, and demonstrated that increased solar wind electric field and pressure resulted in larger currents, with a larger electric field also being associated with an equatorward expansion of the current ovals, consistent with observations using AMPERE data (see section 16.3). In this work, the Iridium TLM data were heavily averaged and therefore were considered to considerably underestimate the true currents whereas the SWMF simulation was a specific run for IMF and solar wind conditions of the statistical binning used for the Iridium TLM data. The LFM model has also been combined with the RCM, in order to test how well magnetic perturbations from datasets like AMPERE can be assimilated into the LFM-RCM model, with the results indicating that such an approach is feasible for the future [*Merkin et al*., 2016].

The SWMF was used in a case study of a geomagnetic storm, giving good agreement with currents derived from Iridium TLM observations and reproducing a rotation in R2 current toward noon with a rotation of the ring current toward the dusk during the storm main phase [*Zaharia et al*., 2010]. The R2 current system had previously been modeled in the storm main phase, using ion and pressure distributions computed from the High Energy Neutral Atom (HENA) data from the IMAGE spacecraft, with magnetic perturbations found to be well modeled on the nightside, as opposed to results from MHD models [*Brandt et al*., 2004]. Further research on the R2 current system was conducted using the Comprehensive Ring Current Model (CRCM), which reproduced the rotation in R2 current during geomagnetically active times and which reported that the distribution of R2 current in latitude and local time changed depending on whether polar cap potential, ionospheric conductivity, or plasma sheet density was enhanced [*Zheng et al*., 2006].

A recent study comparing results of the three MHD simulations run for the Space Weather Prediction Center (SWPC) storm challenge events has also been done to critically assess the relative capabilities of different models to reflect the storm-time dynamics as represented by AMPERE results [*Anderson et al*., 2017]. Two of the five SWPC challenge storms occurred after January 2010 and the AMPERE results for these storms, 4–5 April 2010 and 5–6 August 2011, showed that the total Birkeland current in the simulations could range from a factor of three below to a factor of three greater than the AMPERE results, with LFM and SWMF generally underestimating the current whereas the Open Geospace General Circulation Model (OpenGGCM) generally overestimated the current. Detailed comparison with the distributions of current revealed that, in general, the models and AMPERE differed substantially as indicated by linear regression between the radial current densities evaluated on the same latitude/longitude grids. The regression coefficients were generally between 0 and 0.5 and averaged around 0.25. The SWPC challenge simulations used low resolution codes and the results of *Merkin et al*. [2013] with the higher resolution codes demonstrate that the low resolution codes are not generally capable of reproducing the currents as determined by AMPERE.

16.8. THE FUTURE WITH AMPERE

AMPERE data have been used with SuperDARN data to look at global effects of solar wind and magnetosphere phenomena many times since Iridium data became

available [e.g., *Waters et al*., 2004], and further work combining these two datasets will give the community unparalleled views of the behavior of magnetosphere-ionosphere coupling, but these are not the only two global datasets that can be used in combination. The recent development of the SuperMAG dataset [*Gjerloev*, 2009, 2012] has already unlocked new science, both alone and in combination with AMPERE [e.g., *Laundal et al*., 2015], and the new development of a global fit to SuperMAG data similar to that of the original work on AMPERE will enable science to be done with a complete view of the magnetic perturbations above and below the aurora [*Waters et al*., 2015]. Furthermore, combinations of data both from the ground and above the aurora will lead to more reliable maps of the ionospheric electrodynamics, meaning that the last 6 yr of global Birkeland current maps may be the precursor to a new age of reliable, global views of the electrodynamic ionosphere [*Cousins et al*., 2015b; *Lu*, 2016; *Matsuo et al*., 2015].

Recent work with AMPERE has suggested that there may be an asymmetry between Birkeland current flow in the two hemispheres [*Coxon et al*., 2016a], and work will be needed in the future both to better quantify this asymmetry and to explore phenomena related to Birkeland current in order to examine the origin of such an asymmetry [*Laundal et al*., 2016]. Additionally, it is clear that the resolution of the current systems at work on Earth's nightside is a pressing concern for the community, with no real consensus on the morphology of the current systems in this area (as evidenced by section 16.4), and authors have noted that this should be a priority [*Liemohn et al*., 2016]. Open questions abound concerning the nature of the exact morphology of the Birkeland currents [e.g., *Anderson et al*., 2005; *Milan et al*., 2015], the link between Birkeland current and aurora [*Carter et al*., 2016], and the nature of Birkeland current saturation [*Anderson and Korth*, 2007].

Combining AMPERE data with other datasets, whether via AMIE or similar procedures, or using new techniques of inverting the electrodynamics of the high-latitude ionosphere, promises to be of great utility for a wide range of investigations of Earth's space environment. The availability of nearly continuous 24/7 data coverage offers unprecedented opportunities for coordination with ongoing missions, including Cluster, MMS, and Van Allen Probes making observations in the magnetosphere as well as TIMED and the DMSP satellites making complementary low-altitude observations. The future NASA missions ICON and GOLD missions target middle- and low-latitude thermospheric dynamics and require knowledge of the high-latitude drivers of the global ionosphere and thermosphere that AMPERE can play a key role in providing, and missions making measurements of currents on smaller scales will provide vital information at the other end of the scale. The future of AMPERE beyond the 2017 time frame rests with the Iridium NEXT constellation, which is the planned second generation of the Iridium Constellation. We expect it to yield higher quality input data and hence higher fidelity data products for an even wider array of scientific studies than those to which it has already been applied.

ACKNOWLEDGMENTS

John C. Coxon was funded on NERC grant NE/L007177/1 and STFC Ernest Rutherford grant ST/L002809/1, while Stephen E. Milan was funded on STFC consolidated grant ST/N000749/1. Support for AMPERE has been provided under NSF sponsorship under grants ATM-0739864 and AGS-1420184. We are greatly indebted to the contribution of Iridium Communications for providing the data for AMPERE. The AMPERE data used in this review and the papers cited herein are available at http://ampere.jhuapl.edu/. The authors would like to thank the AGU and the conveners of the AGU Chapman Conference on Currents in Geospace in Dubrovnik, Croatia, and John C. Coxon acknowledges the NSF for a travel grant that enabled him to attend.

REFERENCES

Akasofu, S. I., and C. I. Meng (1969), A study of polar magnetic substorms, *J. Geophys. Res*., *74* (1), 293–313; doi:10.1029/JA074i001p00293.

Anderson, B., and H. Korth (2007), Saturation of global field aligned currents observed during storms by the Iridium satellite constellation, *J. Atmos. Solar Terr. Phys*., *69* (1–2), 166–169; doi: 10.1016/j.jastp.2006.06.013.

Anderson, B. J., C. T. Russell, R. J. Strangeway, F. Plaschke, W. Magnes, D. Fischer, H. Korth, et al. (2016), Electrodynamic context of magnetopause dynamics observed by magnetospheric multiscale, *Geophys. Res. Lett*., *43* (12), 5988–5996; doi: 10.1002/2016GL069577.

Anderson, B. J., H. Korth, C. L. Waters, D. L. Green, and P. Stauning (2008), Statistical Birkeland current distributions from magnetic field observations by the Iridium constellation, *Ann. Geophys*., *26* (3), 671–687; doi:10.5194/angeo-26-671-2008.

Anderson, B. J., H. Korth, C. L. Waters, D. L. Green, V. G. Merkin, R. J. Barnes, and L. P. Dyrud (2014), Development of large-scale Birkeland currents determined from the Active Magnetosphere and Planetary Electrodynamics Response Experiment, *Geophys. Res. Lett*., *41* (9), 3017–3025; doi:10.1002/2014GL059941.

Anderson, B. J., H. Korth, D. T. Welling, V. G. Merkin, M. J. Wiltberger, J. Raeder, R. J. Barnes, et al. (2017), Comparison of predictive estimates of high-latitude electrodynamics with observations of global-scale Birkeland currents, *Space Weather*; doi:10.1002/2016SW001529.

Anderson, B. J., K. Takahashi, and B. A. Toth (2000), Sensing global Birkeland currents with IridiumR engineering magnetometer data, *Geophys. Res. Lett*., *27* (24), 4045–4048; doi:10.1029/2000GL000094.

Anderson, B. J., K. Takahashi, T. Kamei, C. L. Waters, and B. A. Toth (2002), Birkeland current system key parameters derived from Iridium observations: Method and initial validation results, *J. Geophys. Res. Space Physics*, *107* (A6), SMP 11-1–SMP 11-13; doi:10.1029/2001JA000080.

Anderson, B. J., S.-I. Ohtani, H. Korth, and A. Ukhorskiy (2005), Storm time dawn dusk asymmetry of the large-scale Birkeland currents, *J. Geophys. Res. Space Physics*, *110* (A12); doi:10.1029/2005JA011246.

Birkeland, K. (1908), *The Norwegian Aurora Polaris Expedition 1902–1903*, vol. *1*, H. Aschelhoug & Co., Christiania, Norway.

Birkeland, K. (1913), *The Norwegian Aurora Polaris Expedition 1902–1903*, vol. *2*, H. Aschelhoug & Co., Christiania, Norway.

Boakes, P. D., R. Nakamura, M. Volwerk, and S. E. Milan (2014), ECLAT Cluster spacecraft magnetotail plasma region identifications (2001–2009), *Dataset Papers in Science*, *2014* (11), 1–13.

Brandt, P., E. C. Roelof, S.-I. Ohtani, D. G. Mitchell, and B. J. Anderson (2004), IMAGE/HENA: Pressure and current distributions during the 1 October 2002 storm, *Adv. Space Res*., *33* (5), 719–722; doi:https://doi.org/10.1016/S0273-1177(03)00633-1.

Burke, W. J., G. R. Wilson, C. S. Lin, F. J. Rich, J. O. Wise, and M. P. Hagan (2011), Estimating Dst indices and exospheric temperatures from equatorial magnetic fields mea sured by DMSP satellites, *J. Geophys. Res. Space Physics*, *116* (A1); doi:10.1029/2010JA015310, a01205.

Carter, J. A., S. E. Milan, J. C. Coxon, M.-T. Walach, and B. J. Anderson (2016), Average field-aligned current configuration parameterized by solar wind conditions, *J. Geophys. Res. Space Physics*, *121* (2), 1294–1307; doi:10.1002/2015JA021567.

Chisham, G., M. P. Freeman, G. A. Abel, W. A. Bristow, A. Marchaudon, J. M. Ruohoniemi, and G. J. Sofko (2009), Spatial distribution of average vorticity in the high-latitude ionosphere and its variation with interplanetary magnetic field direction and season, *J. Geophys. Res. Space Physics*, *114* (A9); doi: 10.1029/2009JA014263.

Clauer, C. R., and R. L. McPherron (1974), Mapping the local time-universal time development of magnetospheric substorms using mid-latitude magnetic observations, *J. Geophys. Res*., *79* (19), 2811–2820; doi:10.1029/JA079i019p02811.

Clausen, L. B. N., J. B. H. Baker, J. M. Ruohoniemi, S. E. Milan, and B. J. Anderson (2012), Dynamics of the region 1 Birkeland current oval derived from the Active Magnetosphere and Planetary Electrodynamics Response Experiment (AMPERE), *J. Geophys. Res.*, *117*, A06,233.

Clausen, L. B. N., J. B. H. Baker, J. M. Ruohoniemi, S. E. Milan, J. C. Coxon, S. Wing, S. Ohtani, and B. J. Anderson (2013a), Temporal and spatial dynamics of the regions 1 and 2 Birkeland currents during substorms, *J. Geophys. Res. Space Physics*, *118* (6), 3007–3016; doi:10.1002/jgra.50288.

Clausen, L. B. N., J. I. Moen, K. Hosokawa, and J. M. Holmes (2016), GPS scintillations in the high latitudes during periods of dayside and nightside reconnection, *J. Geophys. Res. Space Physics*, *121* (4), 3293–3309; doi:10.1002/2015JA022199.

Clausen, L. B. N., S. E. Milan, J. B. H. Baker, J. M. Ruohoniemi, K.-H. Glassmeier, J. C. Coxon, and B. J. Anderson (2013b), On the influence of open magnetic flux on substorm intensity: Ground- and space-based observations, *J. Geophys. Res. Space Physics*, *118* (6), 2958–2969; doi:10.1002/jgra.50308.

Cnossen, I., and M. Förster (2016), North-south asymmetries in the polar thermosphere ionosphere system: Solar cycle and seasonal influences, *J. Geophys. Res. Space Physics*, *121* (1), 612–627; doi:10.1002/2015JA021750.

Connors, M., and G. Rostoker (2015), Inverting magnetic meridian data using nonlinear optimization, *Earth Planet Space*, *67* (1), 155; doi:10.1186/s40623-015-0315-y.

Connors, M., C. T. Russell, X. Chu, and R. L. McPherron (2015), The February 24, 2010 substorm: A refined view involving a pseudo breakup/expansive phase/poleward bound ary intensification sequence, *Earth Planet Space*, *67* (1), 195; doi:10.1186/s40623-015-0363-3.

Connors, M., R. L. McPherron, B. J. Anderson, H. Korth, C. T. Russell, and X. Chu (2014), Electric currents of a substorm current wedge on 24 February 2010, *Geophys. Res. Lett*., *41* (13), 4449–4455; doi:10.1002/2014GL060604.

Cousins, E. D. P., T. Matsuo, A. D. Richmond, and B. J. Anderson (2015a), Dominant modes of variability in large-scale Birkeland currents, *J. Geophys. Res. Space Physics*; doi:10.1002/2014JA020462.

Cousins, E. D. P., T. Matsuo, and A. D. Richmond (2015b), Mapping high-latitude ionospheric electrodynamics with SuperDARN and AMPERE, *J. Geophys. Res. Space Physics*; doi:10.1002/2014JA020463.

Cowley, S. W. H. (2000), Magnetosphere-ionosphere interactions: A tutorial review, in *Magnetospheric Current Systems*, Geophysical Monograph Series, 118, edited by S.-I. Ohtani, R. Fujii, M. Hesse, and R. L. Lysak, 91–106, American Geophysical Union, Washington, DC, USA.

Cowley, S. W. H., and M. Lockwood (1992), Excitation and decay of solar wind-driven flows in the magnetosphere-ionosphere system, *Ann. Geophys*., *10*, 103–115.

Coxon, J. C., C. M. Jackman, M. P. Freeman, C. Forsyth, and I. J. Rae (2016b), Identifying the magnetotail lobes with Cluster magnetometer data, *J. Geophys. Res. Space Physics*, *121* (2), 1436–1446; doi:10.1002/2015JA022020.

Coxon, J. C., I. J. Rae, C. Forsyth, C. M. Jackman, R. C. Fear, and B. J. Anderson (2017), Birkeland currents during substorms: Statistical evidence for a region 2 intensification after onset and a local reduction in density before onset, *J. Geophys. Res. Space Physics*; doi:10.1002/2017JA023967.

Coxon, J. C., S. E. Milan, J. A. Carter, L. B. N. Clausen, B. J. Anderson, and H. Korth (2016a), Seasonal and diurnal variations in AMPERE observations of the Birkeland currents compared to modeled results, *J. Geophys. Res. Space Physics*, *121* (5), 4027–4040; doi:10.1002/2015JA022050.

Coxon, J. C., S. E. Milan, L. B. N. Clausen, B. J. Anderson, and H. Korth (2014a), The magnitudes of the regions 1 and 2 Birkeland currents observed by AMPERE and their role in solar wind-magnetosphere-ionosphere coupling, *J. Geophys. Res. Space Physics*, *119* (12), 9804–9815; doi:10.1002/2014JA020138.

Coxon, J. C., S. E. Milan, L. B. N. Clausen, B. J. Anderson, and H. Korth (2014b), A superposed epoch analysis of the regions

1 and 2 Birkeland currents observed by AMPERE during substorms, *J. Geophys. Res. Space Physics*, *119* (12), 9834–9846; doi:10.1002/2014JA020500.

Eriksson, S., M. R. Hairston, F. J. Rich, H. Korth, Y. Zhang, and B. J. Anderson (2008), High-latitude ionosphere convection and Birkeland current response for the 15 May 2005 magnetic storm recovery phase, *J. Geophys. Res. Space Physics*, *113* (A3); doi:10.1029/2008JA013139,a00A08.

Förster, M., and S. Haaland (2015), Interhemispheric differences in ionospheric convection: Cluster EDI observations revisited, *J. Geophys. Res. Space Physics*, *120* (7), 5805–5823; doi:10.1002/2014JA020774.

Forsyth, C., A. N. Fazakerley, I. J. Rae, C. E. J. Watt, K. Murphy, J. A. Wild, T. Karlsson, et al. (2014), In situ spatiotemporal measurements of the detailed azimuthal substructure of the substorm current wedge, *J. Geophys. Res. Space Physics*, *119* (2), 927–946; doi:10.1002/2013JA019302.

Fukushima, N. (1969), Equivalence in ground geomagnetic effect of Chapman-Vestine's and Birkeland-Alfven's electric current-systems for polar magnetic storms, *Report of Ionosphere and Space Research in Japan*, *23*, 219–227.

Fukushima, N. (1976), Generalized theorem for no ground magnetic effect of vertical currents connected with Pedersen currents in the uniform-conductivity ionosphere, *Report of Ionosphere and Space Research in Japan*, *30* (1), 35–40.

Ganushkina, N. Y., M. W. Liemohn, S. Dubyagin, I. A. Daglis, I. Dandouras, D. L. De Zeeuw, Y. Ebihara, et al. (2015), Defining and resolving current systems in geospace, *Ann. Geophys.*,*33* (11), 1369–1402; doi:10.5194/angeo-33-1369-2015.

Gjerloev, J. W. (2009), A global ground-based magnetometer initiative, *Eos, Transactions American Geophysical Union*, *90* (27), 230–231; doi:10.1029/2009EO270002.

Gjerloev, J. W. (2012), The SuperMAG data processing technique, *J. Geophys. Res. Space Physics*, *117* (A9); doi:10.1029/2012JA017683.

Green, D. L., C. L. Waters, B. J. Anderson, and H. Korth (2009), Seasonal and inter915 planetary magnetic field dependence of the field-aligned currents for both northern and southern hemispheres, *Ann. Geophys.*, *27* (4), 1701–1715; doi:10.5194/angeo-27-1701-2009.

Green, D. L., C. L. Waters, B. J. Anderson, H. Korth, and R. J. Barnes (2006), Comparison of large-scale Birkeland currents determined from Iridium and SuperDARN data, *Ann. Geophys.*, *24* (3), 941–959; doi:10.5194/angeo-24-941-2006.

Green, D. L., C. L. Waters, H. Korth, B. J. Anderson, A. J. Ridley, and R. J. Barnes (2007), Technique: Large-scale ionospheric conductance estimated from combined satellite and ground-based electromagnetic data, *J. Geophys. Res. Space Physics*, *112* (A5); doi:10.1029/2006JA012069,a05303.

Iijima, T., and T. A. Potemra (1976), The amplitude distribution of field-aligned currents at northern high latitudes observed by Triad, *J. Geophys. Res.*, *81*, 2165–2174.

Iijima, T., and T. A. Potemra (1978), Large-scale characteristics of field-aligned currents associated with substorms, *J. Geophys. Res.*, *83*, 599–615.

Kleiber, W., B. Hendershott, S. R. Sain, and M. Wiltberger (2016), Feature-based validation of the Lyon-Fedder-Mobarry magnetohydrodynamical model, *J. Geophys. Res. Space Physics*, *121* (2), 1192–1200; doi:10.1002/2015JA021825.

Knipp, D. J., A. D. Richmond, G. Crowley, O. de la Beaujardire, E. Friis-Christensen, D. S. Evans, J. C. Foster, I. W. McCrea, F. J. Rich, and J. A. Waldock (1989), Electrodynamic patterns for September 19, 1984, *J. Geophys. Res. Space Physics*, *94* (A12), 16,913–16,923; doi:10.1029/JA094iA12p16913.

Knipp, D. J., T. Matsuo, L. Kilcommons, A. Richmond, B. Anderson, H. Korth, R. Redmon, B. Mero, and N. Parrish (2014), Comparison of magnetic perturbation data from LEO satellite constellations: Statistics of DMSP and AMPERE, *Space Weather*, *12* (1), 2–23; doi:10.1002/2013SW000987.

Korth, H., B. J. Anderson, and C. L. Waters (2010), Statistical analysis of the dependence of large-scale Birkeland currents on solar wind parameters, *Ann. Geophys.*, *28* (2), 515–530; doi:10.5194/angeo-28-515-2010.

Korth, H., B. J. Anderson, H. U. Frey, and C. L. Waters (2005), High-latitude electromagnetic and particle energy flux during an event with sustained strongly northward IMF, *Ann. Geophys.*,*23* (4), 1295–1310; doi:10.5194/angeo-23-1295-2005.

Korth, H., B. J. Anderson, H. U. Frey, T. J. Immel, and S. B. Mende (2004a), Conditions governing localized high-latitude dayside aurora, *Geophys. Res. Lett.*, *31* (4); doi:10.1029/2003GL018911,l04806.

Korth, H., B. J. Anderson, J. G. Lyon, and M. Wiltberger (2008b), Comparison of Birkeland current observations during two magnetic cloud events with mhd simulations, *Ann. Geophys.*, *26* (3), 499–516; doi:10.5194/angeo-26-499-2008.

Korth, H., B. J. Anderson, J. M. Ruohoniemi, H. U. Frey, C. L. Waters, T. J. Immel, and D. L. Green (2008a), Global observations of electromagnetic and particle energy flux for an event during northern winter with southward interplanetary magnetic field, *Ann. Geophys.*, *26* (6), 1415–1430; doi:10.5194/angeo-26-1415-2008.

Korth, H., B. J. Anderson, M. J. Wiltberger, J. G. Lyon, and P. C. Anderson (2004b), Intercomparison of ionospheric electrodynamics from the iridium constellation with global MHD simulations, *J. Geophys. Res. Space Physics*, *109* (A7); doi:10.1029/2004JA010428, a07307.

Korth, H., L. Rastätter, B. J. Anderson, and A. J. Ridley (2011), Comparison of the observed dependence of large-scale Birkeland currents on solar wind parameters with that obtained from global simulations, *Ann. Geophys.*, *29* (10), 1809–1826; doi: 10.5194/angeo-29-1809-2011.

Korth, H., Y. Zhang, B. J. Anderson, T. Sotirelis, and C. L. Waters (2014), Statistical relationship between large-scale upward field-aligned currents and electron precipitation, *J. Geophys. Res. Space Physics*, *119* (8), 6715–6731; doi: 10.1002/2014JA019961.

Laundal, K. M., C. C. Finlay, and N. Olsen (2016), Sunlight effects on the 3D polar current system determined from low Earth orbit measurements, *Earth Planet Space*, *68* (1), 142; doi:10.1186/s40623-016-0518-x.

Laundal, K. M., S. E. Haaland, N. Lehtinen, J. W. Gjerloev, N. Østgaard, P. Tenfjord, J. P. Reistad, et al. (2015), Birkeland current effects on high-latitude ground magnetic field perturbations, *Geophys. Res. Lett.*, *42* (18), 7248–7254; doi:10.1002/2015GL065776.

Le, G., H. Lühr, B. J. Anderson, R. J. Strangeway, C. T. Russell, H. Singer, J. A. Slavin, et al. (2016), Magnetopause erosion during the 17 March 2015 magnetic storm: Combined

field-aligned currents, auroral oval, and magnetopause observations, *Geophys. Res. Lett*., *43* (6), 2396–2404; doi:10.1002/2016GL068257.

Liemohn, M. W., N. Y. Ganushkina, R. M. Katus, D. L. De Zeeuw, and D. T. Welling (2013), The magnetospheric banana current, *J. Geophys. Res. Space Physics*, *118* (3), 1009–1021; doi:10.1002/jgra.50153.

Liemohn, M. W., N. Y. Ganushkina, R. Ilie, and D. T. Welling (2016), Challenges associated with near-Earth nightside current, *J. Geophys. Res. Space Physics*, *121* (7), 6763–6768; doi:10.1002/2016JA022948.

Liou, K., P. T. Newell, B. J. Anderson, L. Zanetti, and C.-I. Meng (2005), Neutral composition effects on ionospheric storms at middle and low latitudes, *J. Geophys. Res. Space Physics*, *110* (A5); doi:10.1029/2004JA010840, a05309.

Lu, G. (2016), Large scale high-latitude ionospheric electrodynamic fields and currents, *Space Sci. Rev*., 1–20; doi:10.1007/s11214-016-0269-9.

Lu, G., M. E. Hagan, K. Husler, E. Doornbos, S. Bruinsma, B. J. Anderson, and H. Korth (2014), Global ionospheric and thermospheric response to the 5 April 2010 geomagnetic storm: An integrated data-model investigation, *J. Geophys. Res. Space Physics*, *119* (12), 10,358–10,375; doi:10.1002/2014JA020555.

Lyons, L. R., B. Gallardo-Lacourt, S. Zou, J. M. Weygand, Y. Nishimura, W. Li, M. Gkioulidou, et al. (2016), The 17 March 2013 storm: Synergy of observations related to electric field modes and their ionospheric and magnetospheric effects, *J. Geophys. Res. Space Physics*, *121* (11), 10,880–10,897; doi: 10.1002/2016JA023237.

Marsal, S. (2015), Conductivities consistent with Birkeland currents in the ampere-driven tie-gcm, *J. Geophys. Res. Space Physics*, *120* (9), 8045–8065; doi: 10.1002/2015JA021385.

Marsal, S., A. D. Richmond, A. Maute, and B. J. Anderson (2012), Forcing the tie-gcm model with Birkeland currents from the active magnetosphere and planetary electrodynamics response experiment, *J. Geophys. Res. Space Physics*, *117* (A6); doi:10.1029/2011JA017416.

Matsui, H., P. J. Erickson, J. C. Foster, R. B. Torbert, M. R. Argall, B. J. Anderson, J. B. Blake, et al. (2016), Dipolarization in the inner magnetosphere during a geomagnetic storm on 7 October 2015, *Geophys. Res. Lett*., *43* (18), 9397–9405; doi:10.1002/2016GL070677.

Matsuo, T., D. J. Knipp, A. D. Richmond, L. Kilcommons, and B. J. Anderson (2015), Inverse procedure for high-latitude ionospheric electrodynamics: Analysis of satellite borne magnetometer data, *J. Geophys. Res. Space Physics*, *120* (6), 5241–5251; doi:10.1002/2014JA020565.

McPherron, R. L., C. T. Russell, and M. P. Aubry (1973), Satellite studies of magnetospheric substorms on August 15, 1968: 9. phenomenological model for substorms, *J. Geophys. Res*., *78* (16), 3131–3149; doi:10.1029/JA078i016p03131.

Merkin, V. G., B. J. Anderson, J. G. Lyon, H. Korth, M. Wiltberger, and T. Motoba (2013), Global evolution of Birkeland currents on 10 min timescales: Mhd simulations and observations, *J. Geophys. Res. Space Physics*, *118* (8), 4977–4997; doi:10.1002/jgra.50466.

Merkin, V. G., D. Kondrashov, M. Ghil, and B. J. Anderson (2016), Data assimilation of low-altitude magnetic perturbations into a global magnetosphere model, *Space Weather*, *14* (2), 165–184; doi:10.1002/2015SW001330.

Merkin, V. G., J. G. Lyon, B. J. Anderson, H. Korth, C. C. Goodrich, and K. Papadopoulos (2007), A global MHD simulation of an event with a quasi-steady northward IMF component, *Ann. Geophys*., *25* (6), 1345–1358; doi:10.5194/angeo-25-1345-2007.

Milan, S. E. (2013), Modeling Birkeland currents in the expanding/contracting polar cap paradigm, *J. Geophys. Res. Space Physics*, *118* (9), 5532–5542; doi: 10.1002/jgra.50393.

Milan, S. E., A. Grocott, C. Forsyth, S. M. Imber, P. D. Boakes, and B. Hubert (2009), A superposed epoch analysis of auroral evolution during substorm growth, onset and recovery: Open magnetic flux control of substorm intensity, *Ann. Geophys*., *27* (2), 659–668; doi:10.5194/angeo-27-659-2009.

Milan, S. E., J. A. Carter, H. Korth, and B. J. Anderson (2015), Principal component analysis of Birkeland currents determined by the Active Magnetosphere and Planetary Electrodynamics Response Experiment, *J. Geophys. Res. Space Physics*, *120* (12), 10,415–10,424; doi:10.1002/2015JA021680.

Milan, S. E., L. B. N. Clausen, J. C. Coxon, J. A. Carter, M.-T. Walach, K. Laundal, N. Østgaard, et al. (2017), Overview of solar wind-magnetosphere-ionosphere-atmosphere coupling and the generation of magnetospheric currents, *Space Sci. Rev*., *206* (1), 547–573; doi:10.1007/s11214-017-0333-0.

Moen, J., and A. Brekke (1993), The solar flux influence on quiet time conductances in the auroral ionosphere, *Geophys. Res. Lett*., *20* (10), 971–974; doi: 10.1029/92GL02109.

Motoba, T., S. Ohtani, B. J. Anderson, H. Korth, D. Mitchell, L. J. Lanzerotti, K. Shiokawa, M. Connors, C. A. Kletzing, and G. D. Reeves (2015), On the formation and ori1051 gin of substorm growth phase/onset auroral arcs inferred from conjugate space-ground observations, *J. Geophys. Res. Space Physics*, *120* (10), 8707–8722; doi: 10.1002/2015JA021676.

Murphy, K. R., I. R. Mann, I. J. Rae, C. L. Waters, B. J. Anderson, D. K. Milling, H. J. Singer, and H. Korth (2012), Reduction in field-aligned currents preceding and local to auroral substorm onset, *Geophys. Res. Lett*., *39* (15); doi: 10.1029/2012GL052798.

Murphy, K. R., I. R. Man, I. Jonathan Rae, C. L. Waters, H. U. Frey, A. Kale, H. J. Singer, B. J. Anderson, and H. Korth (2013), The detailed spatial structure of field aligned currents comprising the substorm current wedge, *J. Geophys. Res. Space Physics*; doi:10.1002/2013JA018979.

Nakamura, R., V. A. Sergeev, W. Baumjohann, F. Plaschke, W. Magnes, D. Fischer, A. Varsani, et al. (2016), Transient, small-scale field-aligned currents in the plasma sheet boundary layer during storm time substorms, *Geophys. Res. Lett*., *43* (10), 4841–4849; doi: 10.1002/2016GL068768.

Papitashvili, V. O., F. Christiansen, and T. Neubert (2002), A new model of field-aligned currents derived from high-precision satellite magnetic field data, *Geophys. Res. Lett*., *29* (14), 28-1–28-4; doi:10.1029/2001GL014207.

Pellinen, R. J., and W. J. Heikkila (1978), Observations of auroral fading before breakup, *J. Geophys. Res. Space Physics*, *83* (A9), 4207–4217; doi: 10.1029/JA083iA09p04207.

Pulkkinen, A., O. Amm, and A. Viljanen (2003), Ionospheric equivalent current distributions determined with the method

of spherical elementary current systems, *J. Geophys. Res. Space Physics*, *108* (A2); doi:10.1029/2001JA005085, 1053.

Reistad, J. P., N. Østgaard, P. Tenfjord, K. M. Laundal, K. Snekvik, S. Haaland, S. E. Milan, K. Oksavik, H. U. Frey, and A. Grocott (2016), Dynamic effects of restoring footpoint symmetry on closed magnetic field lines, *J. Geophys. Res. Space Physics*, *121* (5), 3963–3977; doi:10.1002/2015JA022058.

Richmond, A. D., and Y. Kamide (1988), Mapping electrodynamic features of the high latitude ionosphere from localized observations: Technique, *J. Geophys. Res. Space Physics*, *93* (A6), 5741–5759; doi:10.1029/JA093iA06p05741.

Ritter, P., and H. Lühr (2006), Curl-B technique applied to Swarm constellation for determining field-aligned currents, *Earth Planet Space*, *58* (4), 463–476; doi: 10.1186/BF03351942.

Robinson, R. M., and R. R. Vondrak (1984), Measurements of E region ionization and conductivity produced by solar illumination at high latitudes, *J. Geophys. Res. Space Physics*, *89* (A6), 3951–3956; doi:10.1029/JA089iA06p03951.

Sergeev, V. A., A. V. Nikolaev, M. V. Kubyshkina, N. A. Tsyganenko, H. J. Singer, J. V. Rodriguez, V. Angelopoulos, et al. (2014a), Event study combining magnetospheric and ionospheric perspectives of the substorm current wedge modeling, *J. Geophys. Res. Space Physics*, *119* (12), 9714–9728; doi:10.1002/2014JA020522.

Sergeev, V. A., A. V. Nikolaev, N. A. Tsyganenko, V. Angelopoulos, A. V. Runov, H. J. Singer, and J. Yang (2014b), Testing a two-loop pattern of the substorm current wedge (SCW2L), *J. Geophys. Res. Space Physics*, *119* (2), 947–963; doi:10.1002/2013JA019629.

Sergeev, V. A., N. A. Tsyganenko, M. V. Smirnov, A. V. Nikolaev, H. J. Singer, and W. Baumjohann (2011), Magnetic effects of the substorm current wedge in a spread-out wire model and their comparison with ground, geosynchronous, and tail lobe data, *J. Geophys. Res. Space Physics*, *116* (A7); doi:10.1029/2011JA016471.

Shukhtina, M. A., E. I. Gordeev, V. A. Sergeev, N. A. Tsyganenko, L. B. N. Clausen, and S. E. Milan (2016), Magnetotail magnetic flux monitoring based on simultaneous solar wind and magnetotail observations, *J. Geophys. Res. Space Physics*, *121* (9), 8821–8839; doi:10.1002/2016JA022911.

Siscoe, G. L., and T. S. Huang (1985), Polar cap ination and deation, *J. Geophys. Res. Space Physics*, *90* (A1), 543–547; doi:10.1029/JA090iA01p00543.

Sitnov, M. I., N. A. Tsyganenko, A. Y. Ukhorskiy, B. J. Anderson, H. Korth, A. T. Y. Lui, and P. C. Brandt (2010), Empirical modeling of a CIR-driven magnetic storm, *J. Geophys. Res. Space Physics*, *115* (A7); doi:10.1029/2009JA015169, a07231.

Stephens, G. K., M. I. Sitnov, A. Y. Ukhorskiy, E. C. Roelof, N. A. Tsyganenko, and G. Le (2016), Empirical modeling of the storm time innermost magnetosphere using Van Allen probes and THEMIS data: Eastward and banana currents, *J. Geophys. Res. Space Physics*, *121* (1), 157–170; doi:10.1002/2015JA021700.

Stephens, G. K., M. I. Sitnov, J. Kissinger, N. A. Tsyganenko, R. L. McPherron, H. Korth, and B. J. Anderson (2013), Empirical reconstruction of storm time steady magnetospheric convection events, *J. Geophys. Res. Space Physics*, *118* (10), 6434–6456; doi:10.1002/jgra.50592.

Tenfjord, P., N. Østgaard, K. Snekvik, K. M. Laundal, J. P. Reistad, S. Haaland, and S. E. Milan (2015), How the IMF BY induces a BY component in the closed magnetosphere and how it leads to asymmetric currents and convection patterns in the two hemispheres, *J. Geophys. Res. Space Physics*, *120* (11), 9368–9384; doi:10.1002/2015JA021579.

Waters, C. L., B. J. Anderson, and K. Liou (2001), Estimation of global field-aligned currents using the Iridium R System magnetometer data, *Geophys. Res. Lett.*, *28* (11), 2165–2168; doi:10.1029/2000GL012725.

Waters, C. L., B. J. Anderson, R. A. Greenwald, R. J. Barnes, and J. M. Ruohoniemi (2004), High-latitude Poynting flux from combined Iridium and SuperDARN data, *Ann. Geophys.*, *22* (8), 2861–2875; doi:10.5194/angeo-22-2861-2004.

Waters, C. L., J. W. Gjerloev, M. Dupont, and R. J. Barnes (2015), Global maps of ground magnetometer data, *J. Geophys. Res. Space Physics*, *120* (11), 9651–9660; doi:10.1002/2015JA021596.

Wilder, F., D. G. Crowley, B. J. Anderson, and A. D. Richmond (2012), Intense dayside Joule heating during the 5 April 2010 geomagnetic storm recovery phase observed by AMIE and AMPERE, *J. Geophys. Res. Space Physics*, *117* (A5); doi:10.1029/2011JA017262.

Wilder, F. D., S. Eriksson, H. Korth, J. B. H. Baker, M. R. Hairston, C. Heinselman, and B. J. Anderson (2013), Field-aligned current reconfiguration and magnetospheric response to an impulse in the interplanetary magnetic field BY component, *Geophys. Res. Lett.*, *40* (11), 2489–2494; doi:10.1002/grl.50505.

Wiltberger, M., E. J. Rigler, V. Merkin, and J. G. Lyon (2016), Structure of high latitude currents in magnetosphere-ionosphere models, *Space Sci. Rev.*, 1–24; doi: 10.1007/s11214-016-0271-2.

Yue, C., C.-P. Wang, Y. Nishimura, K. R. Murphy, X. Xing, L. Lyons, M. Henderson, V. Angelopoulos, A. T. Y. Lui, and T. Nagai (2015), Empirical modeling of 3d force balanced plasma and magnetic field structures during substorm growth phase, *J. Geophys. Res. Space Physics*, *120* (8), 6496–6513; doi:10.1002/2015JA021226.

Zaharia, S., V. K. Jordanova, D. Welling, and G. Tóth (2010), Self-consistent inner magnetosphere simulation driven by a global mhd model, *J. Geophys. Res. Space Physics*, *115* (A12); doi:10.1029/2010JA015915, a12228.

Zheng, Y., A. T. Y. Lui, M.-C. Fok, B. J. Anderson, P. C. Brandt, T. J. Immel, and D. G. Mitchell (2006), Relationship between Region 2 field-aligned current and the ring current: Model results, *J. Geophys. Res. Space Physics*, *111* (A11); doi:10.1029/2006JA011603.

Zhu, L., R. Schunk, L. Scherliess, and V. Eccles (2012), Importance of data assimilation technique in defining the model drivers for the space weather specification of the high latitude ionosphere, *Radio Science*, *47* (4); doi:10.1029/2011RS004936,rS0L24.

Zmuda, A. J., J. H. Martin, and F. T. Heuring (1966), Transverse magnetic disturbances at 1100 kilometers in the auroral region, *J. Geophys. Res.*, *71*, 5033–5045.

Zou, S., M. B. Moldwin, A. J. Ridley, M. J. Nicolls, A. J. Coster, E. G. Thomas, and J. M. Ruohoniemi (2014), On the generation/decay of the storm-enhanced density plumes: Role of the convection flow and field-aligned ion flow, *J. Geophys. Res. Space Physics*, *119* (10), 8543–8559; doi:10.1002/2014JA020408.